Eur. Phys. J. B **27**, 29–48 (2002)
DOI: 10.1140/epjb/e20020127

THE EUROPEAN PHYSICAL JOURNAL B
EDP Sciences

Dual model for magnetic excitations and superconductivity in UPd_2Al_3

P. Thalmeier[a]

Max-Planck-Institute for Chemical Physics of Solids, 01187 Dresden, Germany

Received 22 October 2001 and Received in final form 28 February 2002

Abstract. The Heavy Fermion state in UPd_2Al_3 may be approximately described by a dual model where two of the three U-$5f$ electrons are in a localized state split by the crystalline electric field into two low lying singlets with a splitting energy $\Delta \simeq 6$ meV. The third $5f$ electron has itinerant character and forms the Heavy Electron bands. Inelastic neutron scattering and tunneling experiments suggest that magnetic excitons, the collective propagating crystal field excitations of the localized $5f$ electrons, mediate superconducting (sc) pairing in UPd_2Al_3. A theory for this novel mechanism is developed within a nonretarded approach. A model for the magnetic exciton bands is analyzed and compared with experiment. The sc pair potential which they mediate is derived and the gap equations are solved. It is shown that this mechanism favors an odd parity state which is nondegenerate due to the combined symmetry breaking by the crystalline electric field and the AF order parameter. A hybrid model including the spin fluctuation contribution to the pairing is also discussed.

PACS. 74.20.Mn Nonconventional mechanisms (spin fluctuations, polarons and bipolarons, resonating valence bond model, anyon mechanism, marginal Fermi liquid, Luttinger liquid, etc.) – 74.20.Rp Pairing symmetries (other than s-wave)

1 Introduction

Among the uranium-based Heavy Fermion (HF) superconductors [1] (sc) unconventional behaviour is the rule rather than the exception. In the canonical intermetallic U-compounds one observes orbitally degenerate sc states with associated double transition [2] and two upper critical field curves as in the case of UPt_3 [3], furthermore coexistence and competition of different unconventinal sc states with a SDW-like state in the U_{1-x},Th_xBe_{13} was reported [4]. In addition URu_2Si_2 shows superconductivity embedded in a region with a yet undetermined hidden order parameter [5]. In all these cases, when antiferromagnetism (AF) is observed it has no well defined long range order and is characterized by a very small moment size of order $10^{-2}\mu_B$ or less. The situation is distinctly different in the compound UPd_2Al_3 [6]. Its normal state is characterized by a specific heat γ-value of 120 mJ/mole K^2 much smaller than observed in the previous compounds, it is therefore of only moderate HF character and is superconducting below $T_c = 1.8$ K. On the other hand it has long range AF order below $T_N = 14.3$ K with much larger moments of almost atomic like size with $\mu = 0.85\mu_B$. This indicates that in addition to the itinerant electrons there must be nearly localized $5f$-electrons present which has recently also been proposed for UPt_3 [7]. They result from the $5f^2$ configuration of the U^{4+} ionic species which is the dominating one in UPd_2Al_3 [8]. This is supported by the temperature dependent susceptibility which shows an extremely strong hexagonal ac-anisotropy with an almost constant χ_c and a much larger $\chi_a(T)$ which is strongly temperature dependent with a typical behaviour known from crystalline electric field (CEF)-split localized $5f$ states with a singlet-(nonmagnetic) ground state and a first excited state at an energy estimated as $\Delta \simeq 6$ meV. Knight shift analysis in the normal state obtained from μSR-experiments confirm the presence of localized $5f$ moments [9]. Since the CEF ground state is a singlet the AF order must be of the induced moment type, *i.e.* due to mixing with the first excited CEF state caused by the inter-site exchange.

The most direct confirmation for this dual nature of $5f$-electrons in UPd_2Al_3 is obtained from inelastic neutron scattering experiments which have been able to identify the collective propagating excitations that originate in CEF excitations of energy Δ and are broadened into a dispersive band usually termed 'magnetic excitons' due to the action of the intersite exchange. These modes extend up to 8 meV and for a wave vector along the hexagonal axis are quite sharp and well defined [10]. More recently it was found [11–13] that at the AF wave vector $\mathbf{Q} = (0, 0, \pi)$ in reduced units (Appendix A) a strong interaction of these collective modes of localized moments with the heavy conduction electrons exists which leads to a resonance-like structure in the dynamical structure

[a] e-mail: thalm@cpfs.mpg.de

function due to a near degeneracy of the exciton mode energy at **Q** and the superconducting gap. Before that tunneling measurements [17] have already shown that strong coupling anomalies in the tunneling current exist in the same energy range where the magnetic excitons at **Q** were found. This has lead to the conclusion that they are indeed the bosonic 'glue' which is responsible for the formation of Cooper pairs in this compound [18]. The argument is quite analogous to the strong coupling conventional electron-phonon superconductors where the phonon spectrum known from inelastic neutron scattering leaves its imprint on the sc tunneling spectrum. UPd_2Al_3 is therefore the first case of an unconventional HF superconductor where a similar comparison has lead to the identification of the pairing mechanism, in this case the pairing is mediated by the exchange of magnetic excitons.

In the present work this novel type of pairing mechanism is investigated in detail. It is different from both the electron-phonon mechanism in conventional superconductors and from the spin fluctuation mechanism which is commonly assumed to be present in the unconventional superconductors with strongly correlated electrons. The former is mediated by slightly damped real frequency bosons (phonons) which do not couple to the spin degrees of freedom, thus allowing only for spin singlet pairs. The latter is mediated by strongly overdamped spin-fluctuations, *i.e.* bosons with purely imaginary frequency which couple to conduction electron spins in a rotationally invariant manner and in principle allow for both spin singlet and triplet pairing. The new pairing mechanism discussed here has distinctly different features: It is mediated by magnetic excitons which are real frequency, propagating bosonic modes that couple to the conduction electron spin, however in a way which explicitly breaks spin rotational invariance due to the presence of the CEF splitting. Together with the effect of the AF order parameter this will lead to a complete splitting of triplet states resulting in nondegenerate odd parity pair states.

It is the aim of this work to study within a generic dual model of $5f$ electrons (Sect. 2) the magnetic exciton bands (Sect. 3) and the associated pair potential (Sect. 4) of this mechanism, incorporating both the localized CEF states which originate from the $5f^2$ configuration of the U^{4+} state of UPd_2Al_3 and the conduction electrons. Furthermore the gap equations and their explicit solutions together with their node line structure for a quasi one dimensional model are discussed explicitly; it is also shown how the presence of the AF background influences the gap structure and lifts the degeneracy (Sect. 5). Finally we discuss a hybrid model including also the usual spin fluctuation contribution (Sect. 6). A summary and outlook is given in Section 7.

2 Basic Hamiltonian for the dual 5f-model

The pronounced susceptibility anisotropy of UPd_2Al_3 with an almost constant χ_c and a strongly temperature dependent $\chi_a(\mathrm{T})$ with a maximum at $T = 50$ K is perhaps the most direct evidence for the presence of localised CEF-states [8]. In fact the $\chi_{a,c}(\mathrm{T})$-dependence was used to extract the hexagonal CEF-scheme in reference [8] where it was concluded that $U^{4+}(5f^2)$ ground state and first excited states are both singlets. However later it was found [16] that this cannot explain the temperature dependence of the staggered magnetisation and a singlet-doublet system was proposed instead. The magnetic excitations are very similar for both CEF systems except for a small difference in their temperature dependence as will be explained in Section 3.2.1. Therefore using the singlet-singlet CEF scheme will be adequate in the following. It has the ground state $|g\rangle$ (0 meV) and excited state $|e\rangle$ ($\Delta = 6$ meV). The value of Δ is obtained from a fit to the experimental excitations (Sect. 4) and is close to the one obtained from the temperature variation of susceptibility and AF order parameter [16]. All higher CEF levels starting at $\sim$10 meV will be neglected. The total Hamiltonian, including the localized part $H_{CEF} + H_{ff}$, the conduction band states (H_c) of the remaining itinerant $5f$-electron and its interaction with localized states (H_{cf}) was introduced in reference [18] as

$$\begin{aligned} H &= H_c + H_{CEF} + H_{ff} + H_{cf} \\ H &= \sum_{\mathbf{k}\sigma} \epsilon_{\mathbf{k}\sigma} c^\dagger_{\mathbf{k}\sigma} c_{\mathbf{k}\sigma} + \Delta \sum_i |\, e\rangle\langle e\,|_i \\ &\quad - \sum_{\langle\langle ij\rangle\rangle} J_{ff}(ij)\mathbf{J}_i\mathbf{J}_j - 2I_0(g-1)\sum_i \mathbf{s}_i\mathbf{J}_i. \end{aligned} \tag{1}$$

Here $\epsilon_{\mathbf{k}\sigma}$ is the dispersion of itinerant electrons described by ($\mathrm{c}_{\mathbf{k}\sigma}$,$\mathbf{s}_i$) creation and spin operators. The real Fermi surface (FS) of UPd_2Al_3 is very complicated involving many sheets [19,20]. Within a model approach a simplification is necessary keeping only the most important FS part which dominates the HF behaviour due to its large area and mass. It has the shape of a slightly corrugated cylinder along the hexagonal c-axis [19,20]. The cylindrical symmetry has further great advantages for the treatment of the superconding gap equations (Sect. 5). It can be modeled by the expression

$$\epsilon_{\mathbf{k}\sigma} = \epsilon_\perp(\mathbf{k}_\perp\sigma) - 2t_\parallel \cos k_z \tag{2}$$

where $\epsilon_\perp(\mathbf{k}_\perp\sigma)$ is the dispersion perpendicular to the c-axis whose precise form is unimportant in the following, the much smaller dispersion parallel to c which is responsible for the corrugation of the FS cylinder is determined by an effective hopping energy $t_\parallel$. The localised $5f$-electrons have a total angular momentum $\mathbf{J}_i$ ($J = 4$). Within the singlet-singlet subspace they can be represented by a pseudospin $\mathbf{S}_i$ ($S = \frac{1}{2}$) with the correspondence

$$J_x = \alpha S_x,\ J_y = \alpha S_y,\ J_z = \epsilon\left(\frac{1}{2} - S_z\right). \tag{3}$$

This means that $\langle e|J_x|g\rangle = -\mathrm{i}\langle e|J_y|g\rangle = \frac{1}{2}\alpha$ and $\langle e|J_z|g\rangle = 0$, *i.e.* inelastic singlet-singlet transitions can only be excited by the transverse operators $J_{x,y}$. This anisotropy is a direct consequence of the hexagonal CEF and ultimately will also be responsible for a spin space anisotropy of the superconducting pair potential (Sect. 4).

The third term describes a possible superexchange $J_{ff} = 4(g-1)^2 t_{ff}^2/U$ between the localised $5f$-electrons due to their remaining finite inter-site hopping t_{ff}. The last term finally represents the exchange interaction which couples the itinerant and localised $5f$-electrons of the dual model. The total effective inter-site exchange between localized $5f$-moments is then given by its Fourier transform as

$$\overleftrightarrow{J}(\mathbf{q}) = \overleftrightarrow{J}_{ff}(\mathbf{q}) + I_0^2(g-1)^2 \overleftrightarrow{\chi'}_0(\mathbf{q})$$
$$\overleftrightarrow{\chi'}_0(\mathbf{q}) = \overleftrightarrow{\chi}_0(\mathbf{q}) - \frac{1}{N}\sum_{\mathbf{q}} \overleftrightarrow{\chi}_0(\mathbf{q}). \quad (4)$$

The first (superexchange) part is naturally of AF type, the second (RKKY) part is in principle determined by the static conduction electron susceptibility $\overleftrightarrow{\chi}_0(\mathbf{q})$. For the FS corresponding to equation (2) there is a nesting property (Fig. 8) which leads also to an AF RKKY term. Therefore $\overleftrightarrow{J}(\mathbf{q})$ is AF with a maximum at $\mathbf{Q}$. In the following $\overleftrightarrow{J}(\mathbf{q})$ will be treated as an empirical quantity to be parametrized by fitting the actually observed magnetic excitations to the theoretical predictions based on the dual Hamiltonian of equation (1).

3 The antiferromagnetic singlet-singlet system

The 'induced' magnetism of singlet-singlet CEF-systems is well studied for Pr-compounds (for a review, see Ref. [21]). Since U^{4+} has also a f^2 electron configuration similar to Pr^{3+} singlet-singlet systems may also exist in U-compounds with rather localised $5f$-states such as UPd_2Al_3. In a singlet-singlet system the ground state is nonmagnetic, *i.e.* $\langle g|\mathbf{J}|g\rangle \equiv 0$. Nevertheless magnetic moments may appear spontaneously at T_N if the effective exchange is strong enough to mix the excited state $|e\rangle$ into the ground state $|g\rangle$. The mixed state $|\tilde{g}\rangle$ will then have nonzero moment due to the nondiagonal matrix element $\alpha = 2\langle e|J_x|g\rangle$. In this case the AF transition is preceded by the softening of a 'magnetic exciton' mode at the AF wave vector ($\mathbf{Q} = (0,0,\pi)$ in UPd_2Al_3).

3.1 Exchange model and origin of induced AF order

The magnetic exciton mode can be interpreted as originating from local CEF-excitations $|g\rangle \leftrightarrow |e\rangle$ with energy Δ which propagate from site to site due to the effective exchange and this process leads to the magnetic exciton dispersion. It is therefore a collective excitation of localized $5f$-CEF states and may be obtained from the second and third term in equation (1) but taking the total effective exchange of equation (4) instead. Within the two singlet subspace this leads to a Hamiltonian

$$H_0 = (\Delta/\epsilon)\sum_i J_z^i - \frac{1}{2}\sum_{\langle ij\rangle} \mathbf{J}_i \overleftrightarrow{J}_{ij} \mathbf{J}_j \quad (5)$$

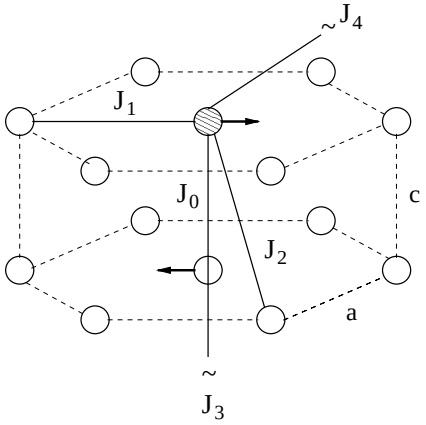

Fig. 1. Schematic view of conventional unit cell of UPd_2Al_3 with only U-atoms shown ($a = 5.35$ Å, $c = 4.185$ Å). Arrows indicate magnetic moments with FM-in plane order and AF stacking along c corresponding to $\mathbf{Q} = (0,0,\frac{\pi}{c})$. The exchange pairs used in the model of Section 3 are also indicated. J_3 and J_4 describe the coupling to n.n.n. pairs along c and in the ab-plane respectively. The values of $J_i (i = 0{-}4)$ are given in the caption of Figure 4.

where $\overleftrightarrow{J}$ is the uniaxial exchange tensor of equation (4) with $J_{ij}^{xx} = J_{ij}^{yy} = J_{ij}^{a}$ and $J_{ij}^{xx} = J_{ij}^{c}$. Its Fourier transform for the two AF sublattices A, B ($= \lambda, \tau$) is given by ($i \in \lambda$)

$$\overleftrightarrow{J}_{\lambda\tau}(\mathbf{q}) = \sum_{j\in\tau} \overleftrightarrow{J}_{ij} \exp(-\mathrm{i}\mathbf{q}(\mathbf{R}_i - \mathbf{R}_j)) = \overleftrightarrow{J}_{\tau\lambda}(\mathbf{q})^*. \quad (6)$$

As mentioned in Section 2 the exchange functions will be empirically parametrized to fit the magnetic exciton dispersion. The exchange couplings included are illustrated in Figure 1. This leads to

$$\overleftrightarrow{J}_D(\mathbf{q}) = \overleftrightarrow{J}_{AA}(\mathbf{q}) = \overleftrightarrow{J}_{BB}(\mathbf{q}) = \overleftrightarrow{J}_1\gamma_1(\mathbf{q}) + \overleftrightarrow{J}_3\gamma_2(\mathbf{q}) + \overleftrightarrow{J}_4\gamma_3(\mathbf{q})$$
$$\overleftrightarrow{J}_N(\mathbf{q}) = \overleftrightarrow{J}_{AB}(\mathbf{q}) = \overleftrightarrow{J}_{BA}(\mathbf{q})^* = [\overleftrightarrow{J}_0 + \overleftrightarrow{J}_2\gamma_1(\mathbf{q})]\gamma_0(\mathbf{q}). \quad (7)$$

The structure functions $\gamma_i(\mathbf{q})$ are given by

$$\gamma_0(\mathbf{q}) = 2\cos q_z$$
$$\gamma_1(\mathbf{q}) = 2\left[\cos q_x + \cos\left(\frac{1}{2}q_x + \frac{\sqrt{3}}{2}q_y\right) + \cos\left(\frac{1}{2}q_x - \frac{\sqrt{3}}{2}q_y\right)\right]$$
$$\gamma_2(\mathbf{q}) = 2\cos 2q_z$$
$$\gamma_3(\mathbf{q}) = 2\left[\cos\sqrt{3}q_y + \cos\frac{\sqrt{3}}{2}(q_y + \sqrt{3}q_x) + \cos\frac{\sqrt{3}}{2}(q_y - \sqrt{3}q_x)\right] \quad (8)$$

where $\gamma_0(q_z \pm Q_z) = -\gamma_0(q_z)$ and $\gamma_2(q_z \pm Q_z) = \gamma_2(q_z)$. This leads to the important symmetries

$\overleftrightarrow{J}_D(q_z \pm Q_z) = \overleftrightarrow{J}_D(q_z)$ and $\overleftrightarrow{J}_N(q_z \pm Q_z) = -\overleftrightarrow{J}_N(q_z)$ where $\mathbf{q}$ and $\mathbf{Q}$=(0,0,π) are given in units of a^{-1} and c^{-1} for x, y and z components, respectively. Each of the exchange parameters $\overleftrightarrow{J}_\nu$ ($\nu = 0{-}4$) in equation (7) which corresponds to a given in- or out-of plane neighbor shell in Figure 1 is in general a uniaxial tensor. The tensor notation will now be suppressed for simplicity. In mean field (mf) approximation the Hamiltonian in equation (5) reads:

$$H_0^{mf} = \sum_i [(\Delta/\epsilon) J_z(i) - h_e^\lambda J_x(i)]$$
$$\mathbf{h}_e^\lambda = [J_{AA}(0) - J_{AB}(0)]\langle J\rangle_\lambda = J(\mathbf{Q})\langle J\rangle_\lambda$$
$$J_e = J(\mathbf{Q}) = 2[3J_1 + 3J_4 + J_3 - J_0 - 6J_2]. \quad (9)$$

Here $\mathbf{h}_e = \mathbf{h}_e(A) = -\mathbf{h}_e(B) = h_e\hat{x}$ is the staggered molecular field and $\langle J\rangle = \langle J_x\rangle = \alpha\langle S_x\rangle$ is the induced moment (in units of gμ_B). The single-ion mf Hamiltonian for each sublattice is then

$$h_0^A(i) = \frac{\Delta}{2}\begin{pmatrix} 1 & -\gamma' \\ -\gamma' & -1 \end{pmatrix}$$
$$h_0^B(i) = \frac{\Delta}{2}\begin{pmatrix} 1 & \gamma' \\ \gamma' & -1 \end{pmatrix} \quad (10)$$

where $\gamma' = \gamma\langle J\rangle$, $\gamma = \frac{\alpha J_e}{\Delta}$. The mf-energies and states are then given by

$$\epsilon_\pm = \pm\frac{\Delta}{2}[1 + \gamma'^2]^{\frac{1}{2}}$$
$$|+\rangle = u|e\rangle - v|g\rangle$$
$$|-\rangle = u|e\rangle + v|g\rangle. \quad (11)$$

Here $u = \cos\theta$, $v = \sin\theta$ determine the rotation to the $|\pm\rangle$ mf eigenstates with $2\theta = \tan^{-1}(\gamma')$, furthermore $\sin 2\theta = (1+\gamma'^2)^{\frac{1}{2}}$ and $\cos 2\theta = \gamma'(1+\gamma'^2)^{\frac{1}{2}}$ where the convention $\theta = \theta_A = -\theta_B$ has been used. From the mf-single ion partition function Z=cosh $\beta\epsilon$ one obtains the mf-equations for the singlet-singlet splitting $\Delta'(T)$ in the ordered state

$$\hat{\Delta}(T) = \frac{\Delta'(T)}{\Delta} = \frac{1}{\Delta}(\epsilon_+ - \epsilon_-) = (1+\gamma'^2)^{\frac{1}{2}}$$
$$\hat{\Delta}(T) = \xi \tanh\left[\left(\frac{\beta\Delta}{2}\right)\hat{\Delta}(T)\right] = 2\xi\langle S\rangle. \quad (12)$$

Here $\langle S_z\rangle \equiv \langle S\rangle$ is the pseudospin expectation value which can be replaced by $\frac{1}{2}$ since $T \ll \Delta$, furthermore $\hat{\Delta}(0) = \frac{1}{2}\alpha\gamma = \xi$. The control parameter of the singlet-singlet system is

$$\xi = \frac{\alpha^2 J_e}{2\Delta} \quad (13)$$

which characterizes the strength of exchange *vs.* size of CEF splitting. It determines the AF transition temperature where $\hat{\Delta}(T_N) = 0$ as

$$T_N = \frac{\Delta}{2\tanh^{-1}(\frac{1}{\xi})} = \frac{\Delta}{2\tanh^{-1}(\frac{2\Delta}{\alpha^2 J_e})}$$
$$\frac{1}{\xi} = \tanh\frac{\Delta}{2T_N}. \quad (14)$$

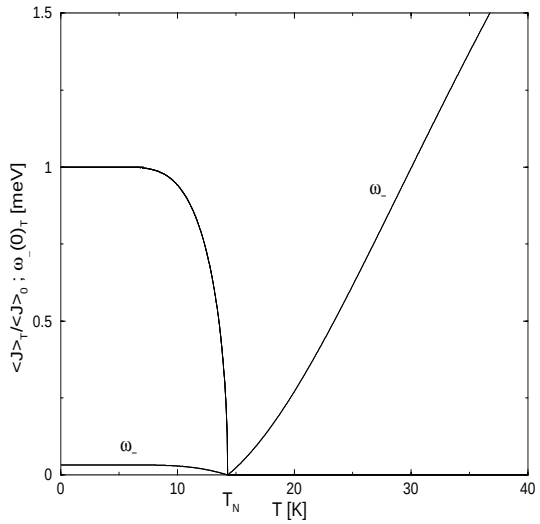

Fig. 2. Temperature dependence of magnetic exciton soft mode frequency $\omega_-(0)_T$ (thin line) (Eq. 33) and normalized induced AF moment $\langle J\rangle_T/\langle J\rangle_0$ (thick line) as given by equation (15). The small finite $\omega_-(0)_T$ below T_N is due to exchange anisotropy. Physical parameters are the same as in Figure 4.

The staggered induced moment as a function of temperature is given by

$$\langle\hat{J}\rangle_T = \frac{\langle J\rangle_T}{\langle J\rangle_0} = (\xi^2-1)^{-\frac{1}{2}}\left[\hat{\Delta}^2(T) - 1\right]^{\frac{1}{2}}$$
$$\langle J\rangle_0 = \alpha\langle S_x\rangle_0 = \frac{1}{2}\alpha\frac{1}{\xi}(\xi^2-1)^{\frac{1}{2}} \quad (15)$$

where $\langle J\rangle_0$ is the saturation moment. To obtain a spontaneous induced moment $\langle J\rangle_0 > 0$ the control parameter ξ must fulfil $\xi > \xi_c \equiv 1$. For $\xi = 1 + \delta$ ($\delta \ll 1$) slightly above its critical value $\xi_c = 1$ the saturation moment is given by

$$\langle J\rangle_0 = \frac{\alpha}{\sqrt{2}}\delta^{\frac{1}{2}};\ \delta = 2\exp\left(-\frac{\Delta}{T_N}\right). \quad (16)$$

Therefore when $\xi \geq 1$ or $T_N \ll \Delta$ the saturation moment becomes exponentially small. This distinguishes an induced moment system from a conventional magnet with degenerate ground state where the saturation moment is a constant independent of T_N. Note that the above relations also hold in the ferromagnetic case if we replace $J_e \to J_{ff}(0) = J_{AA}(0) + J_{AB}(0)$. The temperature dependence of the induced moment is shown in Figure 2.

3.2 Magnetic exciton dispersion and AF soft mode

The local CEF excitation at site i with energy Δ can propagate through the effect of the inter-site exchange whose transverse parts lead to transitions $|e\rangle_i \to |g\rangle_i$ and $|g\rangle_j \to |e\rangle_j$ simultaneously. This causes a widening of Δ into a dispersive band of 'magnetic excitons'. It should

be stressed that these elementary excitations do *not* require the presence of a magnetic order parameter as in the case of spin waves. Magnetic excitons exist already in the paramagnetic (PM) phase. As function of temperature they may exhibit softening at a certain wave vector which signifies a magnetic transition that leads to the appearance of induced moments. This mechanism is well studied for Pr metal [21] and some compounds where the ordering wave vector may be incommensurate in contrast to the commensurate AF wave vector $\mathbf{Q}$ in UPd_2Al_3. In the following a detailed description of the magnetic exciton modes for UPd_2Al_3 is given since they are the bosonic excitations thought to mediate superconductivity in this compound (Sect. 4.2). The calculation is done most conveniently in the linear response formalism in RPA which starts from the dynamical susceptibility of the singlet-singlet system [21].

$$\chi^{\lambda\mu}_{ij;\alpha\beta}(\tau) = -\langle T\{J^{\lambda}_{i\alpha}(\tau)J^{\mu}_{j\beta}(0)\}\rangle \tag{17}$$

where $i,\ j$ = lattice site, λ, μ= AF sublattices (A, B) and $\alpha, \beta = x,\ y,\ z$ are Cartesian coordinates. Its Fourier transform is given in RPA by

$$\overleftrightarrow{\chi}(\mathbf{q},\omega) = \left[1 - \overleftrightarrow{u}(\omega)\overleftrightarrow{J}(\mathbf{q})\right]^{-1}\overleftrightarrow{u}(\omega). \tag{18}$$

Here $\overleftrightarrow{\chi}$, $\overleftrightarrow{u}$ and $\overleftrightarrow{J}$ are 4×4 tensors, *e.g.* $\overleftrightarrow{\chi}$=$\{\chi\}_{\lambda\alpha,\mu\beta}$ with λ, μ = A, B and $\alpha, \beta = x, y$ transverse Cartesian coordinates. The tensor $\overleftrightarrow{u}$ is diagonal in λ, μ and $\overleftrightarrow{J}$ is diagonal in α, β. The expression for $\overleftrightarrow{u}(\omega)$ is given in Appendix (B). To keep it in a simple form in the ordered state ($\langle J\rangle > 0$) a real space back rotation by an angle θ_r= θ^A_r= -θ^B_r has to be applied to compensate for the effect of the molecular field. Under this rotation the exchange tensors transform as

$$\overleftrightarrow{J}'(\lambda\mu) = \overleftrightarrow{D}(\theta^{\lambda}_r)\overleftrightarrow{J}(\lambda\mu)\overleftrightarrow{D}^T(\theta^{\mu}_r). \tag{19}$$

The magnetic exciton modes are then obtained as poles of the dynamical susceptibility in equation (18) leading to the secular equation $\det\overleftrightarrow{\chi}(\mathbf{q},\omega) = 0$ or

$$\left|\overleftrightarrow{u'^{-1}}(\omega) - \overleftrightarrow{J}'(\mathbf{q})\right| = 0. \tag{20}$$

With $\overleftrightarrow{u'^{-1}}(\omega)$ given in equation (B.5). The magnetic exciton branches obtained from the secular equation above will now be discussed for several cases. For brevity the primes in the transformed tensors will be suppressed unless explicitly needed.

3.2.1 Paramagnetic phase, isotropic exchange

In this case there are no sublattices A, B and only one exchange function $\overleftrightarrow{J}(\mathbf{q}) = \overleftrightarrow{J}_D(\mathbf{q}) + \overleftrightarrow{J}_N(\mathbf{q})$ appears, furthermore $\Delta' = \Delta$ holds and equation (20) then yields the PM exciton dispersion

$$\begin{aligned}\omega(\mathbf{q}) &= \Delta - \alpha^2\langle S\rangle J(\mathbf{q})\\ \omega(\mathbf{q}) &= \Delta\left[1 - \frac{\alpha^2 J(\mathbf{q})}{2\Delta}\tanh\frac{\beta}{2}\Delta\right].\end{aligned} \tag{21}$$

At the AF point $\mathbf{Q}$ (PM zone boundary) we have $J(\mathbf{Q}) = J_D(\mathbf{Q}) + J_N(\mathbf{Q}) \equiv J_e$ and therefore

$$\omega(\mathbf{Q},T) = \Delta\left[1 - \xi\tanh\frac{\beta}{2}\Delta\right]. \tag{22}$$

This zone boundary mode in the paramagnetic BZ (PMBZ) becomes soft when $T \to T_N$ from above according to equation (22).

$$\omega(\mathbf{Q},T) = \frac{1}{2}\left(\frac{\Delta}{T_N}\right)^2\left(\xi - \frac{1}{\xi}\right)(T - T_N). \tag{23}$$

It approaches zero linearly above T_N. Below T_N the induced moment of equation (15) appears staggered along the c-axis leading to two AF sublattices A, B. Then $\mathbf{Q} = (0, 0, \pi)$ becomes the new center of the antiferromagnetic BZ (AFBZ). One has the connection $\mathbf{q}\,' = \mathbf{q} - \mathbf{Q}$, where $\mathbf{q} \in$ PMBZ ($|q_z| \le \pi$) and $\mathbf{q}\,' \in$ AFBZ ($|q'_z| \le \frac{\pi}{2}$) as illustrated in the inset of Figure 8. The prime for the AFBZ will be suppressed i.f. unless explicitly necessary. Here it is also appropriate to comment on the use of a singlet-singlet ($|g\rangle, |e\rangle$) low lying CEF system instead of a singlet-doublet scheme ($|g\rangle, |e_{1,2}\rangle$) probably realised in UPd_2Al_3 [16]. For the latter the excitation spectrum within RPA may be obtained from equation (21) by i) a suitably redefined matrix element $\frac{1}{4}\alpha^2$=$\sum_{i=1,2}|\langle e_i|J_x|g\rangle|^2$ in equation (13) and ii) replacing the T-dependent function in equation (21) by $[\tanh\frac{\beta}{2}\Delta]\frac{1}{2}[3 - \tanh\frac{\beta}{2}\Delta]$ which is due to the changed partition function and level occupation caused by the doublet degeneracy. For $T_N \ll \Delta$ the dispersion in the two cases will be almost identical. The inclusion of higher lying degenerate CEF multiplets with diagonal matrix elements would have an interesting effect: Due to their associated Curie terms in the *static* susceptibility which contribute to the AF transition but not to the dynamic susceptibility, the soft mode behaviour will be arrested at a finite frequency at T_N, contrary to the complete softening at T_N for the singlet-singlet case in equation (23). This may be the most important reason for the observed magnetic excitation gap at $\mathbf{Q}$.

3.2.2 AF induced moment phase, isotropic exchange

For the solution of equation (20) one now needs the rotated exchange tensor in equation (19). For isotropic $\overleftrightarrow{J}(\lambda\mu)$ one obtains

$$\begin{aligned}\overleftrightarrow{J}'(\lambda\mu) &= \overleftrightarrow{J}(\lambda\mu)\overleftrightarrow{D}\left(\theta^{\lambda}_r\right)\overleftrightarrow{D}^T(\theta^{\mu}_r)\\ \overleftrightarrow{J}'_D(\mathbf{q}) &= \overleftrightarrow{J}_D(\mathbf{q})\\ \overleftrightarrow{J}'_N(\mathbf{q}) &= \frac{1-\gamma'^2}{1+\gamma'^2}\overleftrightarrow{J}_N(\mathbf{q})\end{aligned} \tag{24}$$

where $\overleftrightarrow{J}'_D(\mathbf{q}), \overleftrightarrow{J}'_N(\mathbf{q})$ are the intra- and inter-sublattice exchange tensors in the rotated ($x',\ y,\ z'$) coordinate system respectively. From equation (20) one then obtains the

magnetic exciton dispersion

$$\omega_{\mp}^2(\mathbf{q}) = [\Delta' - \alpha^2\langle S\rangle(J_D(\mathbf{q}) \mp rJ_N(\mathbf{q}))]$$
$$[\Delta' - \alpha^2\langle S\rangle(J_D(\mathbf{q}) \mp J_N(\mathbf{q}))]$$
$$r = \frac{1-\gamma'^2}{1+\gamma'^2} = \frac{2-\xi^2}{\xi^2}. \quad (25)$$

Here the last identity holds because T$\ll \Delta$ where $\gamma'^2 = \hat{\Delta}^2 - 1 \simeq \xi^2 - 1$. Equivalently this may be written

$$\omega_{\mp}^2(\mathbf{q}) = [\Delta' - \alpha^2\langle S\rangle J_{\pm}(\mathbf{q})]^2 - (\alpha^2\langle S\rangle)^2\gamma'^4\tilde{J}_N^2(\mathbf{q})$$
$$\tilde{J}_N(\mathbf{q}) = (1+\gamma'^2)^{-1}J_N(\mathbf{q});\ J_{\pm}(\mathbf{q}) = J_D(\mathbf{q}) \pm \tilde{J}_N(\mathbf{q}). \quad (26)$$

In the AFBZ $\omega_-(\mathbf{q})$ and $\omega_+(\mathbf{q})$ correspond to acoustic (A) and optical modes (O) respectively. Due to the property $J_N(\mathbf{q} \pm \mathbf{Q}) = -J_N(\mathbf{q})$ the optic mode $\omega_+(\mathbf{q})$ with $\mathbf{q} \in$ AFBZ is the downfolded (shifted by an AF reciprocal lattice vector $\mathbf{Q}$) acoustic mode $\omega_-(\mathbf{q})$ with $\mathbf{q} \in$ PMBZ. This connection is illustrated in Figure 3 (left panel). It is instructive to consider two limiting cases for this dispersion:

(i) $\xi \geq 1$ $(r \to 1)$

In this marginally critical case $r \geq 1$ and equation (25) reduces to

$$\omega_{\mp}^2(\mathbf{q}) = \Delta' - \alpha^2\langle S\rangle J_D(\mathbf{q}) \mp \alpha^2\langle S\rangle J_N(\mathbf{q}). \quad (27)$$

The acoustic mode $\omega_-(\mathbf{q})$ evolves from the paramagnetic soft mode $\omega(\mathbf{q})$ of equation (21) and the optic mode $\omega_+(\mathbf{q})$ is obtained by downfolding $\omega_-(\mathbf{q})$. Therefore we have two strongly split A, O modes in the AFBZ in the present case. Including only n.n. exchange along the c-axis in equation (7) leads to $J_D = 0$ and $J_N(\mathbf{q}) = 2J_0 \cos q_z$ and we obtain with $\alpha^2\langle S\rangle = \xi\Delta \simeq \Delta$:

$$\omega_{\mp}(\mathbf{q}) = \Delta(1 \pm \cos q_z). \quad (28)$$

The two modes are periodic in the reduced AFBZ.

(ii) $\xi \gg 1$ $(r \to -1)$ In this limit the magnetic excitations are exchange dominated and the influence of the CEF is negligible, therefore they can essentially be viewed as AF spin waves. One obtains from equation (25):

$$\omega_{\mp}^2(\mathbf{q}) = [\Delta'^2 - (\alpha^2\langle S\rangle)^2 J_N^2(\mathbf{q})]^{\frac{1}{2}}$$
$$= \alpha^2\langle S\rangle)[J_N^2(0) - J_N^2(\mathbf{q})]^{\frac{1}{2}} \quad (29)$$

where we used $\Delta' = \Delta\xi = \alpha^2\langle S\rangle_0 J_e = \alpha^2\langle S\rangle J_N(0)$. Again, for only n.n. exchange along the c-axis ($J_D = 0$, $J_N(\mathbf{q}) = zJ_0 \cos q_z$, $z = 2$) one obtains

$$\omega_{AF}(\mathbf{q}) = \omega_{\mp}(\mathbf{q}) = \alpha^2\langle S\rangle zJ_0|\sin q_z| = \Delta_{AF}|\sin q_z| \quad (30)$$

which is the spinwave dispersion of a simple AB-antiferrromagnet. Due to isotropic exchange it is twofold degenerate by which it is clearly distinguished from the strongly split A-O exciton modes in the marginally critical ($\xi \geq 1$) case. An illustrative comparison of the two cases ($\xi \geq 1, \xi \gg 1$) is shown in Figure 3 where $\Delta_{AF} = \alpha^2\langle S\rangle zJ_0$ is the spin wave band width with $\Delta_{AF}/\Delta = \xi \gg 1$.

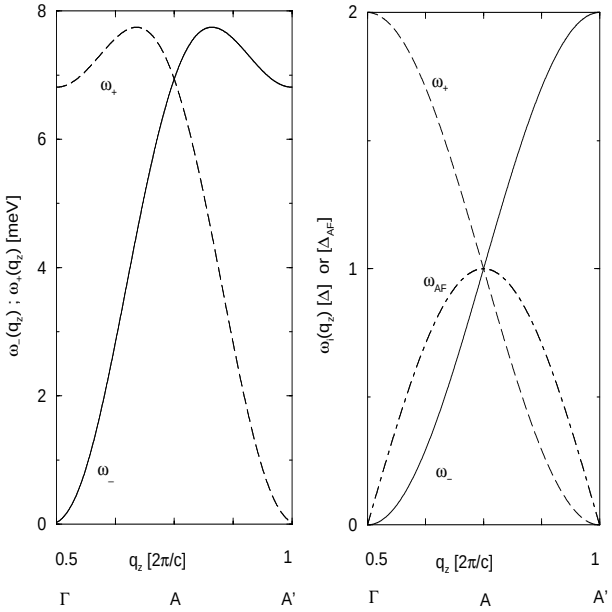

Fig. 3. *Left panel*: Magnetic exciton branches $\omega_\pm$ in the AFBZ (ΓAA$'$ is equivalent to AΓA, see also inset of Figure 8). Physical parameters as in Figure 4. *Right panel*: Simplified model with only n.n exchange along c. Comparison of magnetic exciton branches $\omega_\pm$ for the CEF-dominated case ($\xi \geq 1$) and (twofold degenerate) AF spin wave dispersions ω_{AF} for the exchange dominated case ($\xi \gg 1$), normalization to Δ and Δ_{AF} of equation (30) respectively.

3.2.3 AF phase, anisotropic exchange

In the isotropic case a gapless Goldstone mode for $\mathbf{q} \to 0$ (AFBZ) will be present for any $\xi \geq 1$ above the critical value. However due to the uniaxial symmetry of the effective exchange tensor equation (4) in principle one has to expect gapped magnetic excitations. For simplicity we assume that the anisotropy is independent of the spin pairs, then we may define uniaxial $J_{D,N}^a(\mathbf{q})$, $J_{D,N}^c(\mathbf{q})$ exchange functions in obvious notation where a,c refers to the hexagonal directions. The magnetic exciton modes may again be obtained as solutions of equation (20), however the transformed $\overleftrightarrow{J}'_D(\mathbf{q})$ and $\overleftrightarrow{J}'_N(\mathbf{q})$ are no longer proportional to the unit matrix as in equation (24). Instead one has for the restricted (x', y) coordinate system:

$$\overleftrightarrow{J}'_D = \overleftrightarrow{D}\left(\theta_r^A\right)\overleftrightarrow{J}_D\overleftrightarrow{D}^T\left(\theta_r^A\right) = \begin{pmatrix} u_r^2J_D^a + v_r^2J_D^c & 0 \\ 0 & J_D^a \end{pmatrix} \quad (31)$$

$$\overleftrightarrow{J}'_N = \overleftrightarrow{D}\left(\theta_r^A\right)\overleftrightarrow{J}_N\overleftrightarrow{D}^T\left(\theta_r^B\right) = \begin{pmatrix} u_r^2J_N^a - v_r^2J_N^c & 0 \\ 0 & J_N^a \end{pmatrix} \quad (32)$$

where $u_r = \cos\theta_r$, $v_r = \sin\theta_r$ and the rotation angles for the two sublattices are $\theta_r^A = \theta_r = -2\theta$ and $\theta_r^B = -\theta_r = 2\theta$. Therefore (Appendix B) $u_r = \cos 2\theta = a = (1+\gamma'^2)^{-\frac{1}{2}}$ and $v_r = \sin 2\theta = b = \gamma'$a. From equation (20) and using equations (31, 32) we then obtain the magnetic exciton

modes in the most general case considered here as

$$\begin{aligned}
\omega_{\pm}^2(\mathbf{q}) &= [\Delta' - \alpha^2\langle S\rangle J_{\pm}(\mathbf{q})]^2 - (\alpha^2\langle S\rangle)^2\gamma'^4\tilde{J}(\mathbf{q})_{\pm}^2 \\
J_{\pm}(\mathbf{q}) &= (J_D \pm J_N^{ac}) + (1+\gamma'^2)^{-1}(J_D^{ac} \pm J_N) \\
\tilde{J}_{\pm}(\mathbf{q}) &= (1+\gamma'^2)^{-1}(J_D^{ac} \pm J_N) \\
J_{D,N} &= \frac{1}{2}(J_{D,N}^a + J_{D,N}^c) \\
J_{D,N}^{ac} &= \frac{1}{2}(J_{D,N}^a - J_{D,N}^c). \qquad (33)
\end{aligned}$$

In the case $J_N^a = J_N^c$ and $J_D^a = J_D^c$ this reduces to the isotropic result of equations (25, 26).

3.3 Model calculation, comparison with INS results

The simple AF structure was determined in reference [22] and subsequently inelastic neutron scattering (INS) experiments on single crystalline UPd_2Al_3 were performed [10] in an energy range up to 10 meV in the whole AFBZ to determine the collective magnetic excitations. It was concluded that for $\mathbf{q} \parallel c^*$-axis well defined magnetic excitation modes exist. For $\mathbf{q} \perp c^*$-axis their dispersion was also determined, however line widths are generally larger in this case. An extrinsic damping mechanism *via* coupling to itinerant $5f$-electrons was concluded from the absence of a zone center gap. However later more accurate low energy experiments [11,12] have shown that a gap of 1 meV exists at the AF wave vector (AFBZ zone center). Within the present RPA theory the exchange anisotropy introduced before can only generate small gaps $\leq$0.2 meV because of the vicinity to the quantum critical point at $\xi_c = 1$ of the AF singlet-singlet system as discussed before. As mentioned in Section 3.2.1 a possible origin of the observed gap at the AFBZ zone center is the arrested softening at T_N if the influence of other CEF states on the magnetic ordering is included. Another possibility is a dynamical origin of the gap due to terms neglected in RPA. Finally we mention that the $\mathbf{q} \simeq 0$ low energy excitation modes will be strongly shifted and broadened due to the interaction with $5f$-conduction electrons as proposed and investigated in reference [18].

In the present discussion the focus is on the fundamental origin of the superconducting pair potential and the resulting gap function within the weak coupling approach. For this purpose the details of the low energy spectral behaviour of the soft mode (AFBZ) is not of primary interest. It is more important to obtain a good global description of collective magnetic excitations for all wave vectors and energies since it is the total spectrum which determines the strength and anisotropy of the pairing potential. For this reason we use the RPA theory developed in the previous section to describe the magnetic excitations found in reference [10] for the whole AFBZ. Going beyond RPA for the magnetic exciton spectrum would also necessitate a strong coupling approach to the pairing problem to stay on the same level of theoretical treatment for magnetic and superconducting sub-systems. This challenging problem will be left for a future investigation.

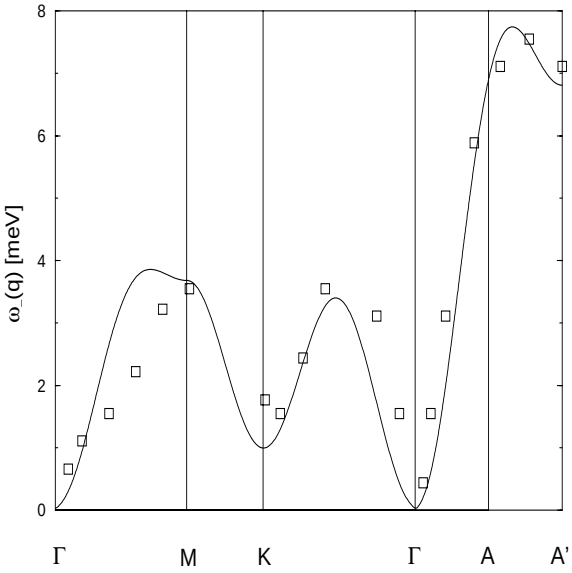

Fig. 4. Magnetic exciton dispersion of UPd_2Al_3 in the hexagonal AFBZ. Squares are data from reference [9]. Solid line: Calculation from equation (33) using the exchange parameters J_i ($i = 0{-}4$) in meV $J_0 = -1.63$, $J_1 = -0.4$, $J_2 = -0.31$, $J_3 = 1.75$ and $J_4 = 0.6$ as defined in Figure 1. For technical reasons an a-c exchange anisotropy of 1.1 is assumed which leads to a very small Γ-point gap.

We will now discuss the experimental and theoretical dispersion of magnetic excitons for UPd_2Al_3 unfolded along typical symmetry lines of the hexagonal AFBZ. For the singlet-singlet system the magnetic exciton dispersion according to equation (33) requires the following quantities: CEF-gap Δ, exchange constants for the various neighbor shells and the uniaxial anisotropy constant. For the CEF splitting we take $\Delta = 6$ meV which corresponds roughly to the center of the magnetic exciton band as seen *e.g.* in the simple model of Section 3.2.2. Furthermore this is also approximately the value obtained from fitting the susceptibility as function of temperature [16]. Since T_N (14.3 K) $\ll \Delta$ (66 K) we are in the CEF dominated regime: According to equation (14) $\xi = (\tanh\frac{\Delta}{2T_N})^{-1} = 1.015$ is only slightly above the value for the QCP at $\xi_c = 1$ which leads to a saturation moment $\langle J\rangle_0 \ll \frac{1}{2}\alpha$ and hence $\Delta' \simeq \Delta$. Therefore the excitation spectrum will be almost like the magnetic excitons in the paramagnetic regime. The exchange model used for the local moments of UPd_2Al_3 is illustrated in Figure 1. A considerable number of neighbor shells has to be included to get an agreeable fit to the experimental data. The result is shown in Figure 4 with the exchange constants in the figure caption corresponding to the notation in Figure 1. The calculated and experimental dispersion are strongest along the hexagonal c-axis where the modes are also well defined *i.e.* the line width is small. In addition it shows a pronounced dip at the K-point. Because of the relation $\omega_+(\mathbf{q} \pm \mathbf{Q}) = \omega_-(\mathbf{q})$ only $\omega_-(\mathbf{q})$ is plotted. In the sector ΓA it corresponds to the acoustic mode and in the sector AA$'$ it is the optical mode, this is illustrated in Figure 3 (left panel). The

large mode energy at A′ gives direct evidence that one has a CEF-dominated singlet-singlet system; in the opposite exchange dominated regime with hypothetical $T_N \gg \Delta$ one would have almost degenerate acoustic and optical branches close to ω_{AF} shown in Figure 3 (right panel) and in this case the excitation energy at A′ should be very small again. It is not entirely clear how realistic the dip at the K-point reported in reference [10] is in view of the fact that the line width becomes much bigger than the mode energy at this symmetry point.

4 The superconducting pair potential

In the known superconductors the formation of Cooper pairs is thought to be mediated by the exchange of bosonic excitations of the medium. This is a simplified picture of a complicated many body problem. More generally the pair formation is the result of a singular behaviour in the low energy part of the two particle scattering matrix. In the simplified picture this singularity is described by the repeated electron-electron scattering *via* boson exchange. In a nonretarded weak coupling approach this is equivalent to the formation of a bound state in the appropriate scattering channel.

Two origins of Cooper pair formation are commonly involved for describing real superconductors: (i) the (BCS) electron-phonon mechanism in conventional superconductors where the effective attraction needed for bound state formation is provided by the exchange of a real frequency (propagating mode) phonon. It is spin independent and allows only for the formation of s-wave spin singlet Cooper pairs. (ii) the spin fluctuation mechanism in strongly correlated electron systems (HF-compounds, cuprates etc.) where the Cooper pair formation is due to exchange of an imaginary frequency spin fluctuation of conduction electrons, predominantly close to an AF zone boundary wave vector (overdamped "anti-paramagnon" mode). The latter mechanism which is in principle relevant also for UPd_2Al_3 , has originally been introduced in the context of superfluid He^3 by Nakajima [23] in its paramagnon form. Later it has been adopted for various Heavy Fermion superconductors by many authors, see *e.g.* reference [24] because it naturally leads to the possibility of unconventional pair states thought to occur in these compounds. It involves the spin degrees of freedom in a rotationally invariant way and allows for spin singlet and triplet pair formation. (iii) As a novel mechanism it has recently been proposed [18] that in U-compounds like UPd_2Al_3 with $5f$-electrons of dual character the exchange of magnetic excitons lies at the origin of superconductivity. This mechanism is distinctly different from those discussed before. On one hand it is mediated by a real frequency propagating mode, the magnetic excitons, on the other hand, as in the previous case it involves the spin variables, but due to the presence of a CEF splitting the rotational symmetry is broken.

In this part of the present work we will derive and discuss the nonretarded effective pair potential of this new mechanism in detail. Because it is important to understand its differences as compared to the spin fluctuation mechanism usually invoked for HF metals we first give a short summary of the salient ingredients of the latter.

4.1 The spin fluctuation model of pairing

This pairing mechanism may be dominant in many strongly correlated electron systems where one has a screened on-site Coulomb interaction of heavy quasiparticles described by

$$H_{int} = I_c \int \mathrm{d}^3 r n_\downarrow(\mathbf{r}) n_\uparrow(\mathbf{r}) = \frac{I_c}{V} \sum_{\mathbf{k},\mathbf{k}'} c^\dagger_{\mathbf{k}\uparrow} c^\dagger_{-\mathbf{k}\downarrow} c_{-\mathbf{k}'\downarrow} c_{-\mathbf{k}'\uparrow}. \quad (34)$$

Summing appropriate two particle scattering diagrams in RPA [23] equation (34) leads to an effective pair Hamiltonian ($\mathbf{q} = \mathbf{k}' - \mathbf{k}$)

$$H_{eff} = \frac{1}{2} \sum_{\mathbf{k}\mathbf{k}',\alpha\beta\gamma\delta} [V_\rho(\mathbf{q})\delta_{\alpha\beta}\delta_{\gamma\delta} + V_s(\mathbf{q})\sigma_{\alpha\beta}\sigma'_{\gamma\delta}] \times c^\dagger_{\mathbf{k}\alpha} c^\dagger_{-\mathbf{k}\gamma} c_{-\mathbf{k}'\delta} c_{\mathbf{k}'\beta} \quad (35)$$

where the sum in parentheses describes the effective two particle interaction and σ, σ' denote Pauli matrices. It contains a spin-independent potential scattering of strength $V_\rho(\mathbf{q})$ and an exchange scattering of strength $V_s(\mathbf{q})$ which are obtained in RPA as

$$V_\rho(\mathbf{q}) = \frac{\frac{1}{2} I_c}{1 + I_c \chi_0(\mathbf{q})}; \qquad V_s(\mathbf{q}) = \frac{-\frac{1}{2} I_c}{1 - I_c \chi_0(\mathbf{q})}. \quad (36)$$

Using the projectors for pair spin singlet ($S = 0$) and triplet ($S = 1$) channels respectively,

$$P_0 = \frac{1}{4}(1 - \sigma\sigma') \qquad P_1 = \frac{1}{4}(3 + \sigma\sigma') \quad (37)$$

with the Kronecker product $(\sigma\sigma')_{\alpha\beta;\gamma\delta} = \sigma_{\alpha\beta}\sigma'_{\gamma\delta}$, one can separate $V_{\mathit{eff}}(\mathbf{q})$ into the irreducible potentials of singlet and triplet Cooper pairing:

$$V_0(\mathbf{q}) = V_\rho(\mathbf{q}) - 3V_s(\mathbf{q}) \simeq \frac{3}{2} I_c^2 \chi(\mathbf{q}) \qquad V_1(\mathbf{q}) = V_\rho(\mathbf{q}) + V_s(\mathbf{q}) \simeq -\frac{1}{2} I_c^2 \chi(\mathbf{q}) \quad (38)$$

where the last approximation in the above equations holds for wave vectors with enhanced spin fluctuations, *i.e.* when $\chi(\mathbf{q}) \gg \chi_0(\mathbf{q})$. Here

$$\chi(\mathbf{q}) = \frac{\chi_0(\mathbf{q})}{1 - I_c \chi_0(\mathbf{q})} \quad (39)$$

is the RPA susceptibility of conduction electrons which has its maximum at a nesting vector $\mathbf{Q}$ which may be the commensurate AF vector. The effective potential may be written, using spin projectors P_0, P_1 and defining the sequence of states as $(\uparrow\uparrow, \uparrow\downarrow, \downarrow\uparrow, \downarrow\downarrow)$, in the following form:

$$\overleftrightarrow{V}_{eff}(\mathbf{q}) = V_0(\mathbf{q})P_0 + V_1(\mathbf{q})P_1 = \begin{pmatrix} V_1 & 0 & 0 & 0 \\ 0 & \frac{1}{2}(V_0+V_1) & -\frac{1}{2}(V_0-V_1) & 0 \\ 0 & -\frac{1}{2}(V_0-V_1) & \frac{1}{2}(V_0+V_1) & 0 \\ 0 & 0 & 0 & V_1 \end{pmatrix} \quad (40)$$

where according to equation (38) $\frac{1}{2}(V_0+V_1) \simeq \frac{1}{2}I_c^2\chi, -\frac{1}{2}(V_0-V_1) \simeq -\frac{1}{2}I_c^2\chi, V_1 \simeq -\frac{1}{2}I_c^2\chi$. Note that the total spin component $s_z = \frac{1}{2}(\sigma_z + \sigma_z')$ is conserved due to rotational invariance of V_{eff}, therefore matrix elements corresponding to a change of the z-component of the pair spin like $\langle\uparrow\uparrow |V_{eff}| \downarrow\downarrow\rangle = \langle\downarrow\downarrow |V_{eff}| \uparrow\uparrow\rangle$ vanish. One may explicitly check by diagonalisation that $V_{eff}(\mathbf{q})$ has singlet $|0\rangle$ and triplet $|1, s_z = 0, \pm 1\rangle$ eigenstates with energies V_0 and V_1 respectively. The momentum dependence of $\chi(\mathbf{q})$ finally determines which orbital pair state will be realized as discussed in reference [24] who conclude that even parity singlet pairs are favored in general.

4.2 Pair potential due to magnetic exciton exchange

In the dual model of equation (1) the on-site Coulomb interaction of the itinerant $5f$-electrons is neglected and only indirect interaction *via* intermediate CEF excitations due to the last term is considered. Since the latter can propagate this means an effective conduction electron interaction *via* the exchange of magnetic excitons. This will now be derived by similar diagrammatic methods as in reference [23], however the details will be quite different for the present case. In this section we neglect the main effect of AF order on the pair potential and consider only the paramagnetic case. For the derivation of the pair potential the Hamiltonian equation (1) will be first rewritten in terms of more convenient bosonic variables for the CEF singlet-singlet excitations introduced *via* the pseudo spin Holstein-Primakoff representation

$$S_i^+ = a_i \;\; S_i^- = a_i^+ \;\; S_i^z = \frac{1}{2} - a_i^+ a_i. \quad (41)$$

Here a_i is a local boson that describes CF-excitations $|g\rangle \to |e\rangle$ at site i. For $T \ll \Delta$ the influence of unphysical states $(a_i)^n|0\rangle$ with $n \geq 2$ is negligible. This condition is very well fulfilled since $T \ll T_N \ll \Delta$. Then the on-site exchange

$$H_{cf} = -2I_0(g-1)\sum_i [s_{iz}J_{iz} + s_i^+ J_i^- + s_i^- J_i^+] \quad (42)$$

can be transformed, using $J_z = \epsilon(\frac{1}{2} - S_z)$ and $J^\pm = \alpha S^\pm$ and equation (1) to obtain

$$H_{cf} = -\frac{I}{\sqrt{N}}\sum_{\mathbf{k}\mathbf{k}'}[c_{\mathbf{k}'\uparrow}^+ c_{\mathbf{k}\downarrow} a_{\mathbf{k}-\mathbf{k}'}^+ + c_{\mathbf{k}'\downarrow}^+ c_{\mathbf{k}\uparrow} a_{\mathbf{k}'-\mathbf{k}}] - \frac{I_z}{\sqrt{N}}\sum_{\mathbf{k}\mathbf{k}'\mathbf{q}}(c_{\mathbf{k}'\uparrow}^+ c_{\mathbf{k}\uparrow} - c_{\mathbf{k}'\downarrow}^+ c_{\mathbf{k}\downarrow}) a_{\mathbf{q}+\mathbf{k}-\mathbf{k}'}^+ a_{\mathbf{q}} \quad (43)$$

where $I = \alpha(g-1)I_0$ and $I_z = \epsilon(g-1)I_0$. For α, ϵ see equation (3), furthermore

$$a_{\mathbf{q}} = \frac{1}{\sqrt{N}}\sum_i a_i e^{i\mathbf{q}\mathbf{R}_i} \quad (44)$$

creates CEF-bosons of momentum $\mathbf{q}$. The total Hamiltonian of equation (1) is then given by

$$H = \sum_{\mathbf{k}\sigma}\epsilon_{\mathbf{k}\sigma}c_{\mathbf{k}\sigma}^\dagger c_{\mathbf{k}\sigma} + \Delta\sum_{\mathbf{q}} a_{\mathbf{q}}^+ a_{\mathbf{q}} + H_{ff} + H_{cf}. \quad (45)$$

The interaction term in equation (43) contains both 1-boson absorption or creation parts as well as 2-boson scattering parts. The latter describes conduction electron scattering from quantum fluctuations in the occupation of the two singlet CEF-states. Its contribution will be neglected in the following discussion. The boson propagator is given by

$$D_{\mathbf{q}}(\tau) = D_{\mathbf{q}}^+(-\tau) = -\langle T_\tau a_{\mathbf{q}}(\tau) a_{\mathbf{q}}^+(0)\rangle \quad (46)$$

and its Fourier transform ($\omega_n = 2n\pi T$) by

$$D_{\mathbf{q}}(i\omega_n) = D_{\mathbf{q}}^+(-i\omega_n) = \frac{1}{i\omega_n - \Delta}\,. \quad (47)$$

The momentum $\mathbf{q}$ for the noninteracting CEF-bosons is a dummy variable. Note that in the zero frequency limit $(D_{\mathbf{q}}D_{\mathbf{q}}^+)_{\omega_n\to 0} = \frac{1}{\Delta^2}$. The lowest order nontrivial polarisation and exchange diagrams for the effective e-e interaction vertex due to the 1-boson part of equation (43) are of order $\sim I^4$ and are shown in Figure 5. For the nonretarded e-e vertex function $\Gamma_0(\mathbf{q})$ that enters the effective pairing Hamiltonian we only need the zero frequency limit of Figure 5 in which the diagrams lead to equal contributions:

$$\Gamma_0^2(\mathbf{q}) = [I^2\chi_0(\mathbf{q},0)]^2(D_{\mathbf{q}}D_{\mathbf{q}}^+)_{\omega_n\to 0} = \left[\frac{I^2}{\Delta}\chi_0(\mathbf{q},0)\right]^2. \quad (48)$$

Here the noninteracting susceptibility $\chi_0(\mathbf{q}) = \chi_{xx}(\mathbf{q}) = \chi_{yy}(\mathbf{q})$ is given by the Lindhard function

$$\chi_0(\mathbf{q}) = \sum_{\mathbf{k}}\frac{f_{\mathbf{k}} - f_{\mathbf{k}+\mathbf{q}}}{\epsilon_{\mathbf{k}+\mathbf{q}} - \epsilon_{\mathbf{k}}}\,. \quad (49)$$

The summation of polarisation and exchange diagrams as in Figure 5 to infinite order in RPA leads to the following nonretarded e-e interaction potential $V_{\alpha\beta\gamma\delta}(\mathbf{q})$ for

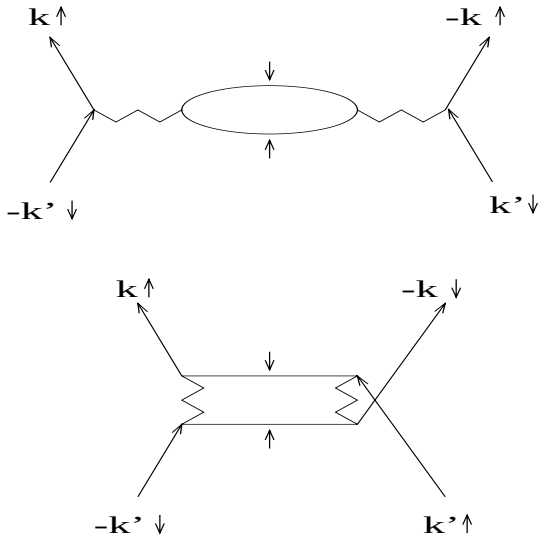

Fig. 5. Lowest order ($\sim I^4$) polarisation diagram (above) with $\mathbf{q} = \mathbf{k}' + \mathbf{k}$ and exchange diagram (below) with $\mathbf{q} = \mathbf{k}' - \mathbf{k}$ contributing to the scattering potentials V_a and V_d of equation (50) respectively. The zig-zag line represents the boson propagator D_0 and the bubble is equal to the conduction electron susceptibility $\chi_0(\mathbf{q})$ in the nonretarded approximation. Small arrows represent conduction electrons spin. Note that the upper diagram describes a process which does not conserve the total pair spin component $(s_z + s'_z)$ leading to a pair potential equation (62) which is not rotationally invariant in spin space. Summation of diagrams of odd order in I^2 leads to V_b and V_c.

the various channels of initial ($\beta\delta$) and final ($\alpha\gamma$) spin configurations:

$$\begin{aligned}
V_a &= V^a_{\downarrow\downarrow,\uparrow\uparrow} = V^a_{\uparrow\uparrow,\downarrow\downarrow} \\
&= -\frac{\chi_0^{-1}\Gamma_0^2}{1-\Gamma_0^2} = -\frac{1}{2}I^2\left[\frac{1}{\Delta(1-\Gamma_0)} - \frac{1}{\Delta(1+\Gamma_0)}\right] \\
V_b &= V^b_{\downarrow\uparrow,\uparrow\downarrow} = V^a_{\uparrow\downarrow,\downarrow\uparrow} \\
&= \frac{I^2 D_0}{1-\Gamma_0^2} = -\frac{1}{2}I^2\left[\frac{1}{\Delta(1-\Gamma_0)} + \frac{1}{\Delta(1+\Gamma_0)}\right] \\
V_c &= V^c_{\downarrow\downarrow,\uparrow\uparrow} = V^c_{\uparrow\uparrow,\downarrow\downarrow} = V_b \\
V_d &= V^d_{\downarrow\uparrow,\uparrow\downarrow} = V^c_{\uparrow\downarrow,\downarrow\uparrow} = V_a. \qquad (50)
\end{aligned}$$

Here $V_a(\mathbf{q})$, $V_b(\mathbf{q})$ with momentum transfer $\mathbf{q} = \mathbf{k} + \mathbf{k}'$ correspond to the polarisation and $V_c(\mathbf{q})$, $V_d(\mathbf{q})$ with $\mathbf{q} = \mathbf{k} - \mathbf{k}'$ to the exchange diagrams of Figure 5. Adding up all contributions and transforming $\mathbf{k} \rightarrow -\mathbf{k}$ in the first two (a, b) terms one obtains the effective e-e interaction Hamiltonian where now $\mathbf{q} = \mathbf{k} - \mathbf{k}'$:

$$\begin{aligned}
&H_{\mathit{eff}} = \\
&\sum_{\mathbf{k}\mathbf{k}'}[V_a(\mathbf{q}) + V_c(\mathbf{q})][c^\dagger_{\mathbf{k}\uparrow}c^\dagger_{-\mathbf{k}\uparrow}c_{-\mathbf{k}'\downarrow}c_{\mathbf{k}'\downarrow} + c^\dagger_{\mathbf{k}\downarrow}c^\dagger_{-\mathbf{k}\downarrow}c_{-\mathbf{k}'\uparrow}c_{\mathbf{k}'\uparrow}] \\
&+ \sum_{\mathbf{k}\mathbf{k}'} V_b(\mathbf{q})[c^\dagger_{\mathbf{k}\downarrow}c^\dagger_{-\mathbf{k}\uparrow}c_{-\mathbf{k}'\downarrow}c_{\mathbf{k}'\uparrow} + c^\dagger_{\mathbf{k}\uparrow}c^\dagger_{-\mathbf{k}\downarrow}c_{-\mathbf{k}'\uparrow}c_{\mathbf{k}'\downarrow}] \\
&+ \sum_{\mathbf{k}\mathbf{k}'} V_d(\mathbf{q})[c^\dagger_{\mathbf{k}\uparrow}c^\dagger_{-\mathbf{k}\downarrow}c_{-\mathbf{k}'\downarrow}c_{\mathbf{k}'\uparrow} + c^\dagger_{\mathbf{k}\downarrow}c^\dagger_{-\mathbf{k}\uparrow}c_{-\mathbf{k}'\uparrow}c_{\mathbf{k}'\downarrow}]. \qquad (51)
\end{aligned}$$

Defining the effective e-e interaction potential by

$$H_{\mathit{eff}} = \frac{1}{2}\sum_{\mathbf{k}\mathbf{k}',\alpha\beta\gamma\delta} V^{\mathit{eff}}_{\alpha\beta\gamma\delta}(\mathbf{q})c^\dagger_{\mathbf{k}\alpha}c^\dagger_{-\mathbf{k}\gamma}c_{-\mathbf{k}'\delta}c_{\mathbf{k}'\beta} \qquad (52)$$

we get the explicit effective interaction matrix by comparison with the previous equation, using $V_\pm = V_a \pm V_b$ and again defining the state sequence as $(\uparrow\uparrow, \uparrow\downarrow, \downarrow\uparrow, \downarrow\downarrow)$:

$$\frac{1}{2}\overleftrightarrow{V}_{\mathit{eff}}(\mathbf{q}) = \begin{pmatrix} 0 & 0 & 0 & V_+ \\ 0 & \frac{1}{2}(V_- + V_+) & -\frac{1}{2}(V_- - V_+) & 0 \\ 0 & -\frac{1}{2}(V_- - V_+) & \frac{1}{2}(V_- + V_+) & 0 \\ V_+ & 0 & 0 & 0 \end{pmatrix}. \qquad (53)$$

Comparison with equation (40) shows that interaction components $V^{\mathit{eff}}_{\uparrow\uparrow\uparrow\uparrow}$ etc. are absent due to the fact that boson absorption or emission always leads to spin flips. On the other hand there are additional components like $V^{\mathit{eff}}_{\uparrow\uparrow\downarrow\downarrow} = V_a + V_b = V_+$ which do not conserve the total pair spin component $s^t_z = (s_z + s'_z)$. Thus magnetic exciton exchange does *not* lead to a rotationally invariant effective pairing potential as in the case of the spin fluctuation mechanism in Section 4.1. This is a direct consequence of the presence of a CEF splitting. The decomposition of $\mathrm{V}_{\mathit{eff}}$ into irreducible contributions as previously given in equation (40) is therefore more involved and will be discussed below.

The static e-e vertex function $\Gamma'_0(\mathbf{q}) = \Gamma'_0(\mathbf{q}) - N^{-1}\sum_{\mathbf{q}}\Gamma_0(\mathbf{q})$ is related to the Fourier transform of the effective exchange interaction $J_{\mathrm{RKKY}}(\mathbf{q})$ of pseudo spins *via* the the relations

$$\begin{aligned}
\alpha^2\langle S\rangle J_{\mathrm{RKKY}}(\mathbf{q}) &= I^2\chi'_0(\mathbf{q}) \\
\Gamma'_0(\mathbf{q}) = \frac{I^2}{\Delta}\chi'_0(\mathbf{q}) &= \frac{\alpha^2\langle S\rangle}{\Delta}J_{\mathrm{RKKY}}(\mathbf{q}) \qquad (54)
\end{aligned}$$

where $\chi'_0(\mathbf{q})$ was given in equation (4, 49). In addition the pseudo spins have a superexchange $J_{ff}(\mathbf{q})$ whose contribution in static RPA limit is described by equivalent diagrams thus leading to a total vertex function

$$\begin{aligned}
&\Gamma(\mathbf{q}) = \Gamma'_0(\mathbf{q}) + \Gamma_{ff}(\mathbf{q}) = \\
&\frac{\alpha^2\langle S\rangle}{\Delta}[J_{\mathrm{RKKY}}(\mathbf{q}) + J_{ff}(\mathbf{q})] \equiv \frac{\alpha^2\langle S\rangle}{\Delta}J(\mathbf{q}). \qquad (55)
\end{aligned}$$

This result may now be substituted in equation (50). As mentioned in Section 2 the total exchange function $J(\mathbf{q})$ will be parametrized by comparison with the experimental exciton dispersion. It has intra-and inter-sublattice parts $J_D(\mathbf{q})$ and $J_N(\mathbf{q})$ respectively with $J(\mathbf{q}) = J_D(\mathbf{q}) + J_N(\mathbf{q})$. Absorbing the constant $\frac{1}{N}\sum_{\mathbf{q}}\Gamma_0(\mathbf{q})$ into a renormalized CEF splitting Δ and replacing $\Delta \rightarrow \Delta'$ for the AF ordered case we then obtain, defining $\omega_R(\mathbf{q}) = 2\Delta' - \omega_-(\mathbf{q})$

$$\begin{aligned}
&\Delta'[1 - \Gamma(\mathbf{q})] = \Delta' - \alpha^2\langle S\rangle J_D(\mathbf{q}) - \alpha^2\langle S\rangle J_N(\mathbf{q}) \equiv \omega_-(\mathbf{q}) \\
&\Delta'[1 + \Gamma(\mathbf{q})] = \Delta' + \alpha^2\langle S\rangle J_D(\mathbf{q}) + \alpha^2\langle S\rangle J_N(\mathbf{q}) \equiv \omega_R(\mathbf{q}). \qquad (56)
\end{aligned}$$

Here $\omega_-(\mathbf{q})$ is nothing but the excitonic dispersion branch which becomes soft at the zone boundary $\mathbf{Q}$ of the PMBZ at T_N and evolves into the acoustic branch with its minimum at the new Γ-point of the AFBZ as explained in Section 3. Note that the energy $\omega_R(\mathbf{q}) = 2\Delta' - \omega_-(\mathbf{q})$ does *not* correspond to an excitation branch. Since $2\Delta' \gg \omega_-(\mathbf{q})$ for all realistic cases $\omega_R(\mathbf{q})$ will never be small and $\omega_R(\mathbf{q})^{-1}$ is regular throughout the AFBZ. Using equation (56) the effective potentials of equation (58) can now be written as

$$V_a = -\frac{I^2}{2}\left[\frac{1}{\omega_-(\mathbf{q})} - \frac{1}{\omega_R(\mathbf{q})}\right]$$
$$V_b = -\frac{I^2}{2}\left[\frac{1}{\omega_-(\mathbf{q})} + \frac{1}{\omega_R(\mathbf{q})}\right]. \qquad (57)$$

Inserting this result into the interaction matrix of equation (53) the possible irreducible pair potentials (*i.e.* the eigenvalues V_κ, $\kappa = 0,\ u,\ v,\ w$ of $\overleftrightarrow{V}_{eff}$) are given by

$$V_0 = (V_a - V_b) = I^2\frac{1}{\omega_R(\mathbf{q})}$$
$$V_u = -(V_a + V_b) = I^2\frac{1}{\omega_-(\mathbf{q})}$$
$$V_v = (V_a + V_b) = -I^2\frac{1}{\omega_-(\mathbf{q})}$$
$$V_w = (V_a + V_b) = -I^2\frac{1}{\omega_-(\mathbf{q})} \qquad (58)$$

with the correspondence $V_0 = V_-$, $V_u = -V_v = -V_w = V_+$ to equation (53). The pair states obtained as eigenstates from equation (53) are classified according to their $s_z = \uparrow\downarrow$ $(= \pm\frac{1}{2})$ quantum numbers. Later on when the effect of AF order is considered, a representation with $s_x = +, -(= \pm\frac{1}{2})$ may be useful. It is obtained by $|+\rangle = R_y(\frac{\pi}{2})|\uparrow\rangle$ etc. where $R_y = \frac{1}{\sqrt{2}}(1 - \mathrm{i}\sigma_y)$ is a rotation by $\frac{\pi}{2}$ around the y-axis. Therefore we also give the relation between the two notations for the eigenstates ψ_κ or ψ^x_κ which correspond to $V_\kappa, \kappa = 0,\ u,\ v,\ w$:

$$\psi_0 = \psi^x_0 = \frac{1}{\sqrt{2}}(|\uparrow\downarrow\rangle - |\downarrow\uparrow\rangle)$$
$$\psi_u = -\psi^x_w = \frac{1}{\sqrt{2}}(|\uparrow\uparrow\rangle - |\downarrow\downarrow\rangle)$$
$$\psi_v = \psi^x_v = \frac{1}{\sqrt{2}}(|\uparrow\uparrow\rangle + |\downarrow\downarrow\rangle)$$
$$\psi_w = \psi^x_u = \frac{1}{\sqrt{2}}(|\uparrow\downarrow\rangle + |\downarrow\uparrow\rangle). \qquad (59)$$

Here ψ_0 describes singlet pairs. In the spin fluctuation model ($\psi_\kappa, \kappa = u,\ v,\ w$) correspond to the degenerate triplet pairs. In the present magnetic exciton model according to equation (58) obviously this degeneracy is partly lifted because the basic Hamiltonian equations (43, 45) is not rotationally invariant in spin space as a result of the coupling to CEF split localized states. The triplet is split into a nondegenerate state ψ_u and a doublet (ψ_v,ψ_w). As a consequence in the present case the irreducible projector representation for the pair potential like equation (53) is different. The projectors to the eigenvectors which satisfy $P_iP_j = P_i\delta_{ij}$ may be written as

$$P_0 = P^x_0 = \frac{1}{4}(1 - \sigma\sigma')$$
$$P_u = P^x_w = \frac{1}{4}(1 - \sigma_x\sigma'_x + \sigma_y\sigma'_y + \sigma_z\sigma'_z)$$
$$P_v = P^x_v = \frac{1}{4}(1 + \sigma_x\sigma'_x - \sigma_y\sigma'_y + \sigma_z\sigma'_z)$$
$$P_w = P^x_u = \frac{1}{4}(1 + \sigma_x\sigma'_x + \sigma_y\sigma'_y - \sigma_z\sigma'_z). \qquad (60)$$

The projector to the doublet subspace $P_D = (P_v + P_w)$ and to the total triplet subspace $P_1 = (P_u + P_v + P_w)$ are given by

$$P_D = \frac{1}{2}(1 + \sigma_x\sigma'_x)$$
$$P_1 = \frac{1}{4}(3 + \sigma\sigma'). \qquad (61)$$

Then similar as in equation (40) $\mathrm{V}_{eff}(\mathbf{q})$ as mediated by magnetic excitons (Eq. (53)) may finally be written as

$$\overleftrightarrow{V}_{eff}(\mathbf{q}) = \frac{I^2}{\omega_R(\mathbf{q})}P_0 + \frac{I^2}{\omega_-(\mathbf{q})}P_u - \frac{I^2}{\omega_-(\mathbf{q})}(P_v + P_w). \qquad (62)$$

There is an intuitively simple interpretation for the CEF-induced triplet splitting present in this model: The conduction electrons can scatter from virtual CEF-excitations Δ only with their s_x (or s_y)-component, therefore the pair states will experience a potential $\sim (I^2/\Delta)(s^{tot}_x)^2$ in lowest order which splits the ($\psi^x_\kappa, \kappa = u,\ v,\ w$) triplet into nondegenerate $\psi^x_w(s^{tot}_x = 0)$ and $\psi^x_u \pm \psi^x_v(s^{tot}_x = \pm 1)$ degenerate pair states.

The previously developed theory of magnetic excitons which explains the experimental observations as shown in Figure 4 can now be used to calculate the pair potential from equations (58, 62). However only the q_x, q_y-averaged potential is needed for the gap equations as explained in the next section.

5 The superconducting gap equations

The effective e-e interaction may lead to a superconducting state with an order parameter given by the gap matrix ($\mathbf{q} = \mathbf{k} - \mathbf{k}'$)

$$\Delta^{\mathbf{k}}_{\alpha\beta} = -\sum_{\mathbf{k}'\gamma\delta} V^{\mathbf{k}-\mathbf{k}'}_{(\alpha\beta),(\gamma\delta)}\langle c_{\mathbf{k}'\gamma}c_{-\mathbf{k}'\delta}\rangle \qquad (63)$$

which satisfies the m.f. gap equation

$$\Delta^{\mathbf{k}}_{\alpha\beta} = -\sum_{\mathbf{k}'\gamma\delta} V^{\mathbf{k}-\mathbf{k}'}_{(\alpha\beta)(\gamma\delta)}\frac{\Delta^{\mathbf{k}'}_{\gamma\delta}}{2E_{\mathbf{k}'}}\tanh\frac{1}{2}\beta E_{\mathbf{k}'}. \qquad (64)$$

Here we defined $V^{\mathbf{k}-\mathbf{k}'}_{(\alpha\beta)(\gamma\delta)} = V^{\mathbf{k}-\mathbf{k}'}_{\alpha\gamma\beta\delta}$ and $(\alpha\beta),(\gamma\delta) = \uparrow\uparrow,\uparrow\downarrow,\downarrow\uparrow,\downarrow\downarrow$ are double spin indices in the notation for s_z-quantisation and $\mathrm{E}_{\mathbf{k}}$ are the superconducting quasiparticle energies. The gap matrix may be decomposed in the canonical way as

$$\overleftrightarrow{\Delta}^{\mathbf{k}} = \mathrm{i}\sum_{i=0}^{3}\sigma_i\sigma_2 d_i^{\mathbf{k}} \tag{65}$$

where $d_0^{\mathbf{k}}$, $\mathbf{d}^{\mathbf{k}} = (d_u^{\mathbf{k}},\ d_v^{\mathbf{k}},\ d_w^{\mathbf{k}})$ correspond to the pair states ψ_0, (ψ_u,ψ_u,ψ_v) respectively introduced before. Explicitly we have the relations in both s_z and s_x quantisation notation:

$$\begin{aligned}
d_0^{\mathbf{k}} &= \frac{1}{2}(\Delta^{\mathbf{k}}_{\uparrow\downarrow} - \Delta^{\mathbf{k}}_{\downarrow\uparrow}) = \frac{1}{2}(\Delta^{\mathbf{k}}_{+-} - \Delta^{\mathbf{k}}_{-+})\\
d_u^{\mathbf{k}} &= -\frac{1}{2}(\Delta^{\mathbf{k}}_{\uparrow\uparrow} - \Delta^{\mathbf{k}}_{\downarrow\downarrow}) = \frac{1}{2}(\Delta^{\mathbf{k}}_{+-} + \Delta^{\mathbf{k}}_{-+})\\
d_v^{\mathbf{k}} &= \frac{1}{2i}(\Delta^{\mathbf{k}}_{\uparrow\uparrow} + \Delta^{\mathbf{k}}_{\downarrow\downarrow}) = \frac{1}{2i}(\Delta^{\mathbf{k}}_{++} + \Delta^{\mathbf{k}}_{--})\\
d_w^{\mathbf{k}} &= \frac{1}{2}(\Delta^{\mathbf{k}}_{\uparrow\downarrow} + \Delta^{\mathbf{k}}_{\downarrow\uparrow}) = -\frac{1}{2}(\Delta^{\mathbf{k}}_{++} - \Delta^{\mathbf{k}}_{--}).
\end{aligned} \tag{66}$$

Using the projector representation equation (62) for the effective potential and the identity

$$\begin{aligned}
P_0\Delta_{\mathbf{k}} &= d_0^{\mathbf{k}}\\
P_\kappa\Delta_{\mathbf{k}} &= d_\kappa^{\mathbf{k}}\hat{d}_\kappa \quad (\kappa \neq 0)
\end{aligned} \tag{67}$$

where $\Delta^{\mathbf{k}} = \{\Delta^{\mathbf{k}}_{(\alpha\beta)}\}$ is a four component vector acted on by the 4×4 projector matrices of equation (60). We then obtain the scalar irreducible gap equations ($\kappa = 0,\ u,\ v,\ w$)

$$\begin{aligned}
d_\kappa^{\mathbf{k}} &= -\sum_{\mathbf{k}'} V_\kappa^{\mathbf{k}-\mathbf{k}'} F_{\mathbf{k}'} d_\kappa^{\mathbf{k}'}\\
F_{\mathbf{k}} &= \frac{1}{2}E_{\mathbf{k}}\tanh\frac{1}{2}\beta E_{\mathbf{k}}\\
E_{\mathbf{k}} &= [(\epsilon_{\mathbf{k}}-\mu)^2 + |d_\kappa^{\mathbf{k}}|^2]^{\frac{1}{2}}.
\end{aligned} \tag{68}$$

Before solving these equations explicitly we note that the gap functions can be classified according to the crystal symmetry group which in this case is the orthorhombic group D_{2h} due to the presence of the AF order parameter with $\mathbf{m_Q} \parallel \hat{x}$. The corresponding irreducible representations of gap functions can be listed as

$$\begin{aligned}
d_0^{\mathbf{k}} &\sim \cos k_z: \quad A_{1g}(\Gamma_1^+)\\
\mathbf{d_k} = (d_u^{\mathbf{k}},0,0) &\sim \hat{x}\sin k_z: \quad B_{2u}(\Gamma_2^-)\\
\mathbf{d_k} = (0,d_v^{\mathbf{k}},0) &\sim \hat{y}\sin k_z: \quad B_{3u}(\Gamma_4^-)\\
\mathbf{d_k} = (0,0,d_w^{\mathbf{k}}) &\sim \hat{z}\sin k_z: \quad A_{1u}(\Gamma_1^-).
\end{aligned} \tag{69}$$

These representations have even ($d_0^{\mathbf{k}}$) and odd ($\mathbf{d}_\kappa^{\mathbf{k}}, \kappa = u,v,w$) parity respectively The basis functions have all odd character with respect to the transformation $\mathbf{k} \to \mathbf{k} \pm \mathbf{Q}$, namely $\mathbf{d}_\kappa^{\mathbf{k}\pm\mathbf{Q}} = -\mathbf{d}_\kappa^{\mathbf{k}}(\kappa = 0,\ u,\ v,\ w)$. In D_{2h} there is no symmetry reason why ($d_v^{\mathbf{k}}$, $d_w^{\mathbf{k}}$) should be degenerate. In fact we show later that the AF order connected with D_{2h} symmetry will lead to a splitting into nondegenerate $d_-^{\mathbf{k}}$ and $d_+^{\mathbf{k}}$ superconducting states.

5.1 Solution of gap equations for cylindrical symmetry

The explicit solution of equation (68) at this stage cannot be performed for the real FS of $\mathrm{UPd_2Al_3}$ which has many complicated sheets [19,20]. Such an attempt would also not be compatible with the very simple nonretarded model potential of equation (58) whose $\mathbf{k}$-dependence is not calculated from the real FS but obtained from parametrizing the experimental magnetic exciton dispersion. Therefore we use the simplified model FS according equation (2) represented by the corrugated cylinder shown schematically in the inset of Figure 8. The cylindrical symmetry of the model FS leads to an important simplification of the gap equations equation (68) which can now be approximated by a one-dimensional integral equation in the variable k_z. This allows one to continue with an analytical treatment. Explicitly then

$$d_\kappa(k_z) = -\sum_{k_z'}\bar{V}_i(k_z-k_z')d_\kappa(k_z')\sum_{k_\perp'}\frac{\tanh\frac{\beta}{2}E(k_\perp',k_z')}{E(k_\perp',k_z')} \tag{70}$$

where $\mathbf{k}_\perp = (k_x,k_y)$, $k_x = k_\perp\cos\phi$, $k_y = k_\perp\sin\phi$ and ϕ is the azimuthal angle in the ab-plane. For the above separation of variables it is assumed that the ϕ-dependence of the order parameter can be neglected, this means we restrict to representations of the type given in equation (69) and higher harmonics. In addition for the cylindrical FS sheet in $\mathrm{UPd_2Al_3}$ $\epsilon(\mathbf{k}_\perp,\sigma)$ depends only on the modulus $k_\perp$. Therefore only the $q_x,\ q_y$-*averaged* pair potentials $\bar{V}_\kappa(q_z)$ appear in the gap equation where we define

$$\bar{V}_\kappa(q_z) = \frac{1}{4\pi^2}\int_{BZ}\mathrm{d}q_x\mathrm{d}q_y V_\kappa(q_x,q_y,q_z). \tag{71}$$

Using the expressions in equation (58) and the calculated exciton dispersion for $\mathrm{UPd_2Al_3}$ in Section 3 we obtain these averaged pair potentials as shown in Figure 6. Because of the singular behaviour of $V_\kappa(\mathbf{q})$ at the AF-point $\mathbf{Q}$ the absolute value of averaged potentials $|\bar{V}_\kappa(q_z)|$ ($\kappa = u,\ v,\ w$) show a pronounced maximum at $\mathbf{Q}$=(0,0,π). On the other hand the averaged singlet pair potential $\bar{V}_0(q_z)$ is rather smooth with a flat maximum for q_z around 0.4π. This is due to the nonsingular nature of $\mathrm{V}_0(\mathbf{q})$ as discussed in Section 4.

The gap equation equation (70) may now be completely factorized by expanding $\bar{V}_\kappa(q_z)(q_z = k_z - k_z')$ in lattice harmonics according to

$$\begin{aligned}
\bar{V}_\kappa(q_z) &= \sum_m \bar{V}_\kappa^m\cos q_z\\
&= \sum_m \bar{V}_\kappa^m(\cos mk_z\cos mk_z' - \sin mk_z\sin mk_z').
\end{aligned} \tag{72}$$

Furthermore we may expand the even ($\kappa = 0$) and odd parity ($\kappa = u,\ v,\ w$) gap functions into

$$d_0(k_z) = \sum_{m\geq 0} d_0^m\cos mk_z; \quad d_\kappa(k_z) = \sum_{m\geq 1} d_\kappa^m\sin mk_z. \tag{73}$$

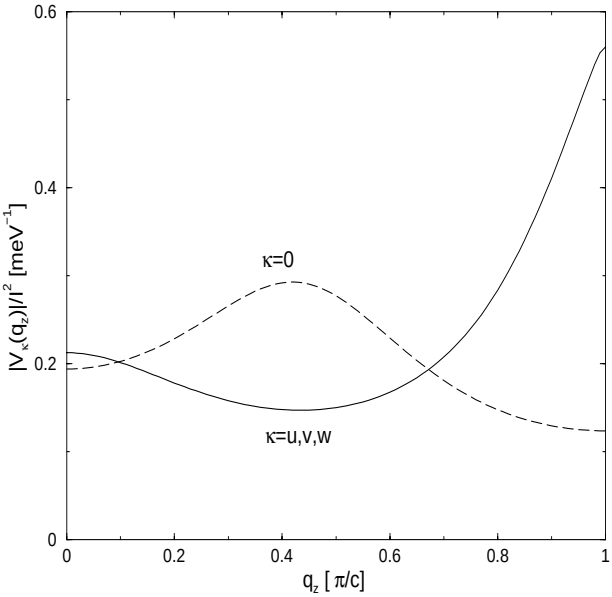

Fig. 6. q_z-dependence of the absolute value of q_x, q_y-averaged pairing potentials $\bar{V}_\kappa$ in the PMBZ for even ($\bar{V}_0 > 0$) and odd ($\bar{V}_u > 0$ and $\bar{V}_v$, $\bar{V}_w < 0$) parity of the gap function. $q_z = 0$ corresponds to the A′-point and $q_z = \frac{\pi}{c}$ to the Γ point of the AFBZ in Figure 4 respectively.

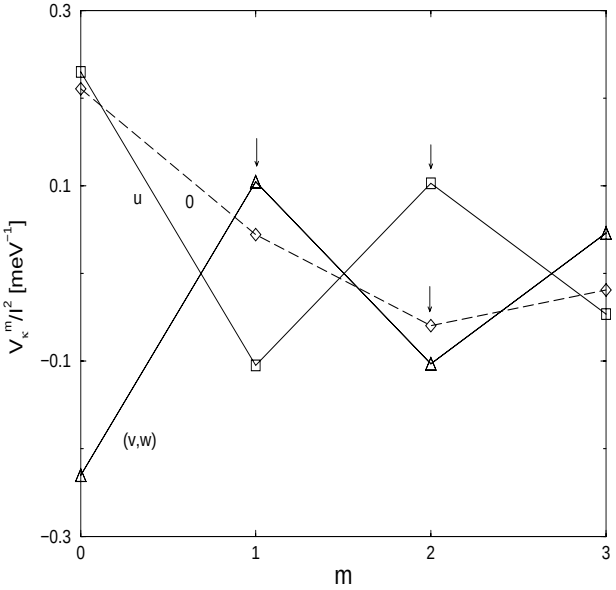

Fig. 7. Fourier components $\bar{V}_\kappa^m$ of $\bar{V}_\kappa(q_z)$ according to equation (72). dashed line (diamonds): $\kappa = 0$, full lines: $\kappa = v$, w (degenerate,triangles) and $\kappa = u$ (squares). The Fourier components with $m \leq 2$ which lead to a nonzero $T_{c\kappa}^m$ in equation (78) have been designated by arrows. The odd parity (v, w) component ($m = 1$) is the most favorable.

The order parameter may now be in general represented as vectors $\mathbf{d}_0 = \{d_0^m\}$ and $\mathbf{d}_\kappa = \{d_\kappa^m\}$ and the gap equations for the components obtained from inserting equations (72, 73) in equation (70) finally can be written as

$$\begin{aligned} 1 &= \sigma_\kappa N(0) \bar{V}_\kappa^m G_m[\mathbf{d}_\kappa] \\ G_m[\mathbf{d}_\kappa] &= \frac{1}{\pi}\int_0^\pi \alpha_m(k_z') F[T, k_z', \mathbf{d}_\kappa] \mathrm{d}k_z' \\ F[T, \mathbf{d}_\kappa(k_z')] &= \int_0^{\omega_-^c} \mathrm{d}\xi \frac{\tanh \frac{1}{2}\beta E(\xi, k_z')}{E(\xi, k_z')} \cdot \end{aligned} \tag{74}$$

Here ω_-^c is the magnetic exciton band cutoff energy, $\sigma_\kappa = -1$ for $\kappa = 0$ and $\sigma_\kappa = 1$ for $\kappa = u,\ v,\ w$. Note that σ_κ is due to the different signs for even and odd parity parts in the harmonic decomposition in equation (72). Furthermore we have for $\kappa = 0$:

$$\begin{aligned} E(\xi, k_z) &= \left[\xi^2 + \left(\sum_n d_\kappa^n \cos n k_z\right)^2\right]^{\frac{1}{2}} \\ \alpha_m(k_z) &= \cos^2(m k_z) \end{aligned} \tag{75}$$

and for $\kappa = u,\ v,\ w$ similar equations

$$\begin{aligned} E(\xi, k_z) &= \left[\xi^2 + \left(\sum_n d_\kappa^n \sin n k_z\right)^2\right]^{\frac{1}{2}} \\ \alpha_m(k_z) &= \sin^2(m k_z). \end{aligned} \tag{76}$$

At the critical temperature T_c, $\mathbf{d}_\kappa = 0$ and equation (74) simplifies to

$$\begin{aligned} F(T_c) &= N(0) \int_0^{\omega_-^c} \frac{\tanh \frac{1}{2}\beta_c \xi}{\xi} \mathrm{d}\xi = N(0) \ln(A \beta_c \omega_-^c) \\ G_m[0] &= \bar{\alpha}_m F(T_c). \end{aligned} \tag{77}$$

Here $A = 1.13$ and $\bar{\alpha}_m$ is the average of $\alpha_m(k_z)$ in the interval [0,π]. One has $\bar{\alpha}_m = 1$ for $\kappa = 0$, $m = 0$ and $\bar{\alpha}_m = \frac{1}{2}$ for $\kappa = 0,\ u,\ v,\ w$ and $m \geq 1$. This leads to the weak coupling BCS- formula for the transition temperature:

$$T_{c\kappa}^m = 1.13(\omega_-^c) \exp\left(-\frac{1}{\bar{\alpha}_m N(0) |\bar{V}_\kappa^m|}\right) \cdot \tag{78}$$

For $T_{c\kappa}^m > 0$ the conditions $\bar{V}_0^m < 0$ for the even $d_0^m (\kappa = 0, m \geq 0)$ singlet and $\bar{V}_\kappa^m > 0$ ($\kappa = u,\ v,\ w, m \geq 1$) for odd parity d_κ^m-states must be satisfied. This difference in the required sign of the Fourier components $\bar{V}_0^m$ can again be traced back to the decomposition in equation (72). The Fourier components in equation (72) with $m = 0 - 4$ are shown in Figure 7. Within the weak coupling approach the sc phase realised is the one with the highest $T_{c\kappa}^m$, *i.e.* the highest $\bar{V}_\kappa^m > 0$ ($\kappa = u, v, w$) or $-\bar{V}_0^m > 0$ ($\kappa = 0$) value. From the calculated values in Figure 7 we notice that the degenerate $\bar{V}_{\kappa=v,w}^{m=1}$ is the most favorable which is slightly larger than $\bar{V}_{\kappa=u}^{m=2}$. The former corresponds to an odd parity doublet

$$\mathbf{d}(k_z) = (d_v^1 \sin k_z, d_w^1 \sin k_z) \tag{79}$$

with $|d_v^1| = |d_w^1|$. It has node lines of the gap at $k_z = 0$. As mentioned before this degeneracy is accidental in

the present model due to the neglect of AF ordering and therefore there is no symmetry determined phase relation between the d_v^1 and d_w^1 amplitudes. The second slightly less favorable odd parity state $d_u^2 \sin 2k_z$ is nondegenerate and has line nodes at $k_z = 0, \frac{\pi}{2}$.

An important conclusion from this analysis is that for the present pure magnetic exciton model the singlet state

$$d_0(k_z) = d_0^1 \cos k_z \tag{80}$$

is not stable because $V_0^1 > 0$ is repulsive instead of attractive as required in this channel. This is due to the fact that the potential $\bar{V}_0(q_z)$ in Figure 6 (dashed line) has its maximum *not* at the PM zone boundary ($q_z = \pi$) but rather close to $q_z = 0.4\pi$. This behaviour can be traced back to the form of $V_0(\mathbf{q})$ in equation (58) which shows that the denominator $2\Delta' - \omega_-(\mathbf{q})$ and not the exciton mode energy $\omega_-(\mathbf{q})$ which leads to the maximum at $q_z = \pi$ for the odd parity state potentials $\bar{V}_\kappa(q_z)$ at $q_z = \pi$ in the PMBZ. This result is robust against the details of the exciton exchange model.

5.2 Effect of AF order on superconducting gap equations

In the previous treatment the influence of AF order on the pair potential was largely neglected. Sofar it only enters through the renormalized singlet-singlet splitting Δ' in the magnetic exciton dispersion which is of minor importance. A much more pronounced effect is due to the competition of sc pair formation and reconstruction of quasiparticle states at the FS by AF long range order. This leads to an important modification of the effective pair potential for wave vectors close to the AF ordering vector $\mathbf{Q}$. This is also known from AF phonon mediated superconductors such as the borocarbides [25,26]. The application of this idea to the present case is formally similar but more involved because of the more general possible pair states as compared to conventional electron-phonon singlet superconductors treated in the above references. In this section we show how AF order modifies the magnetic exciton pair potential of equation (62) and the effect on the sc states as discussed above.

5.2.1 Transformation to magnetic Bloch states

The AF order parameter

$$\langle \mathbf{J}_i \rangle = \langle J \rangle_0 \hat{x} \cos(\mathbf{Q}\mathbf{R}_i) \tag{81}$$

leads to an additional periodic potential for the conduction electrons due to H_{cf} in equation (43) which has twice the period (2c) of the lattice potential (c). It is given by

$$H_{cf}^{mf} = I_0(g-1)\langle J \rangle_0 \sum_{\mathbf{k}} \left(c_{\mathbf{k}+\mathbf{Q}\downarrow}^\dagger c_{\mathbf{k}\uparrow} + c_{\mathbf{k}-\mathbf{Q}\uparrow}^\dagger c_{\mathbf{k}\downarrow} \right) \tag{82}$$

and leads to a reconstruction of the conduction band states (see *e.g.* Refs. [26,27]) which may be described by a unitary transformation to the new *magnetic* Bloch states of the AF lattice given by

$$\begin{aligned} a_{\mathbf{k}1}^\dagger &= \alpha_{\mathbf{k}} c_{\mathbf{k}\uparrow}^\dagger + \beta_{\mathbf{k}} c_{\mathbf{k}+\mathbf{Q}\downarrow}^\dagger \\ a_{\mathbf{k}+\mathbf{Q}2}^\dagger &= \beta_{-\mathbf{k}-\mathbf{Q}} c_{\mathbf{k}\uparrow}^\dagger + \alpha_{-\mathbf{k}-\mathbf{Q}} c_{\mathbf{k}+\mathbf{Q}\downarrow}^\dagger . \end{aligned} \tag{83}$$

The $\alpha_{\mathbf{k}}$, $\beta_{\mathbf{k}}$ are the real *magnetic* transformation coefficients [25,26] below T_N (not to be confused with $u_{\mathbf{k}}$, $v_{\mathbf{k}}$ which transform to the superconducting quasiparticles below T_c). The effect of AF on the pair potential equation (62) is included by expressing the latter with the transformed pair operators $\mathbf{B}_{\mathbf{k}} = \{a_{\mathbf{k}\sigma} a_{-\mathbf{k}\sigma'}, (\sigma\sigma') = 11, 12, 21, 22\}$ instead of the pair operators $\mathbf{b}_{\mathbf{k}} = \{c_{\mathbf{k}\sigma} c_{-\mathbf{k}\sigma'}, (\sigma\sigma') = \uparrow\uparrow, \uparrow\downarrow, \downarrow\uparrow, \downarrow\downarrow\}$ in the paramagnetic state. This transformation $\mathbf{b}_{\mathbf{k}} = T_{\mathbf{k}} \mathbf{B}_{\mathbf{k}}$ is furnished *via* the symmetric 4×4-matrix

$$T_{\mathbf{k}} = \begin{pmatrix} \alpha_{\mathbf{k}}^2 & \alpha_{\mathbf{k}}\beta_{\mathbf{k}} & \alpha_{\mathbf{k}}\beta_{\mathbf{k}} & \beta_{\mathbf{k}}^2 \\ \alpha_{\mathbf{k}}\beta_{\mathbf{k}} & \alpha_{\mathbf{k}}^2 & \beta_{\mathbf{k}}^2 & \alpha_{\mathbf{k}}\beta_{\mathbf{k}} \\ \alpha_{\mathbf{k}}\beta_{\mathbf{k}} & \alpha_{\mathbf{k}}^2 & \beta_{\mathbf{k}}^2 & \alpha_{\mathbf{k}}\beta_{\mathbf{k}} \\ \alpha_{\mathbf{k}}^2 & \alpha_{\mathbf{k}}\beta_{\mathbf{k}} & \alpha_{\mathbf{k}}\beta_{\mathbf{k}} & \beta_{\mathbf{k}}^2 \end{pmatrix} . \tag{84}$$

Then the effective pairing Hamiltonian transforms into ($\mathbf{q} = \mathbf{k}' - \mathbf{k}$)

$$H_{\mathit{eff}} = \frac{1}{2} \sum_{\mathbf{k}\mathbf{k}'} \mathbf{b}_{\mathbf{k}'}^\dagger \overleftrightarrow{V}_{\mathit{eff}}(\mathbf{q}) \mathbf{b}_{\mathbf{k}} = \frac{1}{2} \sum_{\mathbf{k}\mathbf{k}'} \mathbf{B}_{\mathbf{k}'}^\dagger \overleftrightarrow{\hat{V}}_{\mathit{eff}}(\mathbf{q}) \mathbf{B}_{\mathbf{k}} \tag{85}$$

using the projector representation of equation (62) the effective pair potential may be written as

$$\begin{aligned} \overleftrightarrow{\hat{V}}_{\mathit{eff}}(\mathbf{q}) &= T_{\mathbf{k}'} \overleftrightarrow{V}_{\mathit{eff}}(\mathbf{q}) T_{\mathbf{k}}^\dagger \\ &= \sum_\kappa V_\kappa(\mathbf{q}) T_{\mathbf{k}'} P_\kappa T_{\mathbf{k}}^\dagger = \sum_\kappa V_\kappa(\mathbf{q}) \hat{P}_\kappa . \end{aligned} \tag{86}$$

As long as $\mathbf{k}, \mathbf{k}'$ are far away from the AF Bragg planes $\mathbf{k} = \pm\frac{1}{2}\mathbf{Q}$ one has $T_{\mathbf{k}}$, $T_{\mathbf{k}'} \simeq 1$ and $\hat{P}_\kappa \simeq P_\kappa$ still projects to the eigenstates of equation (59). However close to the Bragg planes $\hat{P}_\kappa \neq P_\kappa$ and $\overleftrightarrow{\hat{V}}_{\mathit{eff}}(\mathbf{q})$ and hence the gap equations will be strongly modified. Explicitly we have

$$\begin{aligned} \hat{P}_0 &= a_{\mathbf{k}'} a_{\mathbf{k}} P_0 \\ \hat{P}_u &= a_{\mathbf{k}'} a_{\mathbf{k}} P_u \\ \hat{P}_v &= P_v + b_{\mathbf{k}'} b_{\mathbf{k}} P_w + b_{\mathbf{k}'} P_{vw} + b_{\mathbf{k}} P_{wv} \\ \hat{P}_w &= P_w + b_{\mathbf{k}'} b_{\mathbf{k}} P_v + b_{\mathbf{k}'} P_{vw} + b_{\mathbf{k}} P_{wv} . \end{aligned} \tag{87}$$

Here we defined the transfer operators $P_{vw} = P_{wv}^\dagger = |\psi_v\rangle\langle\psi_w|$ between different pair states. this means that AF order mixes $\psi_v^{\mathbf{k}}$, $\psi_w^{\mathbf{k}}$ states for wave vectors close to the Bragg planes, contrary to $\psi_0^{\mathbf{k}}$, $\psi_u^{\mathbf{k}}$ which stay in the same subspace. The coefficients in equation (87) are related to the magnetic transformation coefficients *via*

$$\begin{aligned} a_{\mathbf{k}} = \alpha_{\mathbf{k}}^2 - \beta_{\mathbf{k}}^2 &= \left[1 + \frac{(I\langle S_x \rangle)^2}{(\epsilon_{\mathbf{k}} - \epsilon_{\mathbf{k}+\mathbf{Q}})^2} \right]^{-\frac{1}{2}} \\ b_{\mathbf{k}} = (1 - a_{\mathbf{k}}^2)^{\frac{1}{2}} = 2\alpha_{\mathbf{k}}\beta_{\mathbf{k}} &= \frac{I\langle S_x \rangle}{|\epsilon_{\mathbf{k}} - \epsilon_{\mathbf{k}+\mathbf{Q}}|} (\alpha_{\mathbf{k}}^2 - \beta_{\mathbf{k}}^2), \end{aligned} \tag{88}$$

where $\mathrm{I}\langle S_x \rangle = I_0(g-1)\langle J \rangle_0$.

5.3 Modified gap equations in the AF state

The above relations enable us to derive the modified sc gap equations in the presence of AF order. The effective pairing of equations (45, 86) leads to gap equations analogous to equation (63) for electrons in magnetic Bloch states:

$$\hat{\Delta}_{\mathbf{k}} = -\sum_{\mathbf{k}'} \hat{V}_{eff}(\mathbf{q})\hat{\Delta}_{\mathbf{k}'} F_{\mathbf{k}'}. \tag{89}$$

Multiplication with a projector P_κ from the left and using the identities $P_v P_{vw} = P_{vw}$, $P_v P_{wv} = 0$ etc. we arrive at the modified gap equations for $\kappa = 0, u$:

$$\begin{aligned} \hat{d}^{\mathbf{k}}_\kappa &= -\sum_{\mathbf{k}'}[a^2_{\mathbf{k}'} V_\kappa(\mathbf{q})]\hat{d}^{\mathbf{k}'}_\kappa F_{\mathbf{k}'} \\ E_{\mathbf{k}} &= [\xi^2_{\mathbf{k}} + d^{\mathbf{k}2}_\kappa]^{\frac{1}{2}} \\ d^{\mathbf{k}}_\kappa &= a_{\mathbf{k}}\hat{d}^{\mathbf{k}}_\kappa = (\alpha^2_{\mathbf{k}} - \beta^2_{\mathbf{k}})\hat{d}^{\mathbf{k}}_\kappa. \end{aligned} \tag{90}$$

This shows that for the $\psi^{\mathbf{k}}_0$, $\psi^{\mathbf{k}}_u$ pair states the effective pair potential in the presence of AF is given by

$$\hat{V}_\kappa(\mathbf{k}-\mathbf{k}') = (\alpha^2_{\mathbf{k}} - \beta^2_{\mathbf{k}})V_\kappa(\mathbf{k}-\mathbf{k}')(\alpha^2_{\mathbf{k}'} - \beta^2_{\mathbf{k}'}) \tag{91}$$

which vanishes at the Bragg planes $\mathbf{k} = \pm\frac{1}{2}\mathbf{Q}$, *i.e.* states which are connected by the AF ordering vector do not contribute to sc pairing. This leads to the well known depression but usually not destruction of superconductivity by AF order, see *e.g.* reference [26]. Far from the magnetic Bragg planes $\hat{V}_\kappa(\mathbf{k}-\mathbf{k}') \simeq V_\kappa(\mathbf{k}-\mathbf{k}')$. Furthermore the gap function entering the quasiparticle energy $E_{\mathbf{k}}$ is $d^{\mathbf{k}}_\kappa$ which has an additional zero for $\mathbf{k} = \pm\frac{1}{2}\mathbf{Q}$ due to the prefactor $(\alpha^2_{\mathbf{k}} - \beta^2_{\mathbf{k}})$. This factor does not change sign at $\mathbf{k} = \pm\frac{1}{2}\mathbf{Q}$ and therefore does not lead to an additional node line. The modified gap equations can now be derived in a similar way for $\kappa = u, v$:

$$\begin{pmatrix} d^{\mathbf{k}}_v \\ d^{\mathbf{k}}_w \end{pmatrix} = -\sum_{\mathbf{k}'} \begin{pmatrix} V_v(\mathbf{q}) & \mathrm{i}b_{\mathbf{k}}V_v(\mathbf{q}) \\ -\mathrm{i}b_{\mathbf{k}}V_w(\mathbf{q}) & V_w(\mathbf{q}) \end{pmatrix} \begin{pmatrix} d^{\mathbf{k}'}_v \\ d^{\mathbf{k}'}_w \end{pmatrix} F_{\mathbf{k}'}. \tag{92}$$

Obviously the two states $(d^{\mathbf{k}}_v,\ d^{\mathbf{k}}_w)$ are mixed at the presence of AF order. According to equation (58) $V_v = V_w \equiv V_D$ and equation (92) can easily be diagonalised. One finally obtains the gap equations for the new eigenstates $(\kappa = +, -)$:

$$\begin{aligned} \hat{d}^{\mathbf{k}}_\pm &= -\sum_{\mathbf{k}'}[(1 \mp b_{\mathbf{k}'})V_D(\mathbf{q})]\hat{d}^{\mathbf{k}'}_\pm F_{\mathbf{k}'} \\ E_{\mathbf{k}} &= [\xi^2_{\mathbf{k}} + d^{\mathbf{k}2}_\kappa]^{\frac{1}{2}} \\ d^{\mathbf{k}}_\pm &= (1 \mp b_{\mathbf{k}})^{\frac{1}{2}}\hat{d}^{\mathbf{k}}_\pm = (1 \mp 2\alpha_{\mathbf{k}}\beta_{\mathbf{k}})^{\frac{1}{2}}\hat{d}^{\mathbf{k}}_\pm \\ d^{\mathbf{k}}_\pm &= \frac{1}{\sqrt{2}}(d^{\mathbf{k}}_v \pm \mathrm{i}d^{\mathbf{k}}_w). \end{aligned} \tag{93}$$

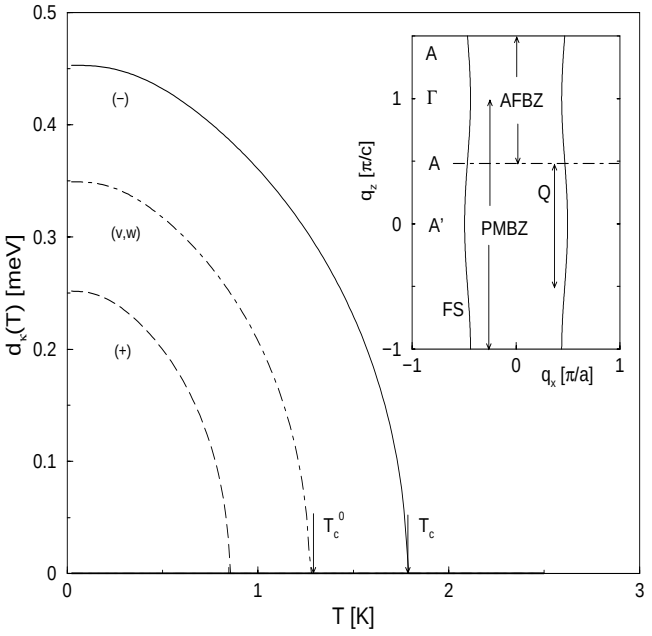

Fig. 8. Temperature dependence of gap function amplitudes $d_-(T)$ (full line) and $d_+(T)$ (dashed line) with AF order effect included (λ_{AF} according to equation (97)). $\Delta\lambda_{sc} = 4.3$ meV is chosen such that $T_c = 1.8$ K. dashed-dotted line: AF moment effect suppressed ($\lambda_{AF} \equiv 0$), with the same λ_{sc}, the transition temperature is then $T^0_c = 1.27$ K. *Inset*: Schematic view of PM Fermi surface (FS) described by equation (2) with PM and AF Brillouin zones indicated. Γ and A′ are the AFBZ and PMBZ zone centers respectively. States on the FS connected by the AF ordering wave vector $\mathbf{Q}$ are reconstructed by the AF order. The model FS shows nesting at wavevectors $(q_x,\ q_y,\ q_x)$ and $(-q_x, -q_y,\ q_z + Q)$.

These equations for ψ_+, ψ_- pair states are formally identical to those for ψ_0, ψ_u in equation (90) however with a different effective pair potential

$$\hat{V}_\pm(\mathbf{k}-\mathbf{k}') = (1 \mp b_{\mathbf{k}})^{\frac{1}{2}} V_D(\mathbf{k}-\mathbf{k}')(1 \mp b_{\mathbf{k}'})^{\frac{1}{2}}\,. \tag{94}$$

At the Bragg planes $b_{\mathbf{k}} \simeq 1$, this implies that the pair potential V_+ for $d^{\mathbf{k}}_+$ is reduced to zero, similar as in the case $\kappa = 0, u$ but for $d^{\mathbf{k}}_-$ the pair potential V_- is enhanced in this region of k-space, therefore AF order supports the sc pairing in the $d^{\mathbf{k}}_-$ state.

As for the PM case in Section 5.1 we will now consider the simple situation of the FS sheet with cylindrical symmetry and small dispersion along c shown in the inset of Figure 8. Then again the gap equations can be decomposed into Fourier components which satisfy equation (74) as in the PM case. However the form factor $\alpha_m(k_z)$ and the quasiparticle energy $E(\xi, k_z)$ are now different because they include the effect of AF order. One obtains

from equations (90, 93)

$$\begin{aligned}
\kappa = 0: \quad & \alpha_m(k_z) = g(k_z)\cos^2(mk_z) \\
& E(\xi, k_z) = \left[\xi^2 + g(k_z)\left(\sum_n d_\kappa^n \cos nk_z\right)^2\right]^{\frac{1}{2}} \\
\kappa = u: \quad & \alpha_m(k_z) = g(k_z)\cos^2(mk_z) \\
& E(\xi, k_z) = \left[\xi^2 + g(k_z)\left(\sum_n d_\kappa^n \sin nk_z\right)^2\right]^{\frac{1}{2}} \\
\kappa = \pm: \quad & \alpha_m(k_z) = h_\kappa(k_z)\cos^2(mk_z) \\
& E(\xi, k_z) = \left[\xi^2 + h_\kappa(k_z)\left(\sum_n d_\kappa^n \sin nk_z\right)^2\right]^{\frac{1}{2}}.
\end{aligned} \tag{95}$$

Here we defined $g(k_z) = a_{\mathbf{k}}^2 = (\alpha_{k_z}^2 - \beta_{k_z}^2)^2$ and $h_\pm(k_z) = (1 \mp 2\alpha_{k_z}\beta_{k_z})$. Using equation (88) one can derive

$$\begin{aligned}
g(k_z) &= \frac{\cos^2 k_z}{\lambda_{AF}^2 + \cos^2 k_z} \\
h_\pm(k_z) &= = 1 \mp [1 - g(k_z)]^{\frac{1}{2}}.
\end{aligned} \tag{96}$$

The functions $g(k_z)$, $h_\pm(k_z)$ with the parameter $\lambda_{AF} \ll 1$ given below account for the influence of AF order on the sc gap *via* the FS reconstruction caused by H_{cf}^{mf} in equation (82). Specifically a finite λ_{AF} will split the degenerate doublet pair state ($d_v^{\mathbf{k}}$, $d_w^{\mathbf{k}}$) of the PM case.

5.4 Numerical solution of gap equations

We now investigate some of the possible solutions of the gap equations quantitatively. It must be kept in mind that this work is based on a model theory which cannot make absolute predictions for the experimentally realised gap function. Its main purpose is a better understanding of the physics of a novel type of pairing mechanism leading to the magnetic exciton mediated superconductivity.

We first give estimates of the physical parameters involved in the present superconducting model for UPd_2Al_3 in addition to those already discussed in Section 3 for the magnetic exciton model itself. According to reference [19] the Fermi level is in the middle of a peak which we approximate by a square DOS of width $W = 2E_F = 0.88$ eV. Assuming one conduction electron per U site we have $N(0) = E_F^{-1} = 0.0023$ meV^{-1} for the model DOS. The small bandwidth $W_\parallel \ll W$ of the k_z dispersion is given by $W_\parallel = 4t_\parallel \simeq 2E_F(A_c^{max}/A_c^{min} - 1)$ where the last approximate relation is obtained assuming a free electron like dispersion $\perp c$ and relating the change of the FS cylinder cross section A_c in the PMBZ along c to the hopping $t_\parallel$. The deviation of the ratio A_c^{max}/A_c^{min} from 1 characterizes the amount of 'corrugation' of the FS cylinder along c as shown in Figure 8, its value is obtained from dHvA experiments [20] as $A_c^{max}/A_c^{min} \simeq 1.24$ in the AFBZ. This leads to an estimate $W_\parallel = 0.21$ eV or $(W_\parallel/W) = 0.24$ consistent with the assumption made above. The interaction H_{cf} between localized $5f$ and conduction electrons with strength $I = \alpha I_0(g-1)$ has two competing effects which are characterized by the dimensionless coupling constants

$$\lambda_{sc} = \frac{N(0)I^2}{\Delta} \quad \lambda_{AF} = \frac{(I/\alpha)\langle J\rangle_0}{W_\parallel}. \tag{97}$$

Whereas λ_{sc} characterizes the strength of the pair potential due to magnetic exciton exchange, λ_{AF} is associated with the effect of AF on the sc pair states. Since both are determined by the interaction constant I they are not independent and one has the relation

$$\lambda_{AF} = \frac{1}{2}\frac{\langle J\rangle_0}{\alpha}\frac{W}{W_\parallel}[N(0)\Delta]^{\frac{1}{2}}\lambda_{sc}^{\frac{1}{2}}. \tag{98}$$

The quantities $W_\parallel/W = 0.24$ and $[N(0)\Delta]^{\frac{1}{2}} = 0.12$ are estimated within our model so that only one independent parameter λ_{sc} remains which will be fixed to achieve the proper $T_c = 1.8$ K. The solution of the gap equation (74) for the AF case of equation (95) proceeds by iteration. As discussed in Section 5.1 the most favorable pair state, judging from the irreducible potentials in Figure 7 is the odd parity doublet given by equation (79).

The temperature variation of its sc amplitudes $d_+(T)$, $d_-(T)$ (i.f. the index $m = 1$ is suppressed) is shown in Figure 8 for two cases: (a) neglect of AF order, setting $\lambda_{AF} \equiv 0$ arbitrarily, then both representations are accidentally degenerate (b) including the effect of AF with the proper λ_{AF} according to equation (98): the degeneracy is lifted due to the finite λ_{AF} and the nondegenerate $d_-^{\mathbf{k}}$ state describes the true sc phase in the AF background. It is preferred as compared to $d_+^{\mathbf{k}}$ due to its gap enhancement factor $(1 + b_{\mathbf{k}})$ in equation (93). The iteration procedure used for the calculation of $d_\kappa(k_z)$ in equation (74) allows for the appearance of different Fourier components below $T_{c\kappa}$ which correspond to V_κ^n irreducible potentials which are smaller than the maximum one with $n = m$. Their appearance would lead to a change of the profile of $d_\kappa(k_z)$ as function of temperature. For all cases studied with the potentials of Figure 7 such a case never appears, therefore in the quasiparticle energies in equation (95) the summation over n can simply be replaced by the dominant term for $n = m$.

In Figure 9 it is shown how the suppression of T_c and the splitting of $d_+^{\mathbf{k}}$, $d_-^{\mathbf{k}}$ representations evolves as function of λ_{sc} due to the effect of λ_{AF} given in equation (96). AF order renders the $d_-^{\mathbf{k}}$ state more favorable. Once $d_-^{\mathbf{k}} > 0$ at T_c the split-off doublet component $d_+^{\mathbf{k}}$ with its lower transition temperature will be completely suppressed by the already finite condensation energy of the $d_-^{\mathbf{k}}$ state. Therefore in the AF background only a single nondegenerate state

$$d_-^{\mathbf{k}} = d_-(T)(1 + 2\alpha_{\mathbf{k}}\beta_{\mathbf{k}})^{\frac{1}{2}}\sin k_z \tag{99}$$

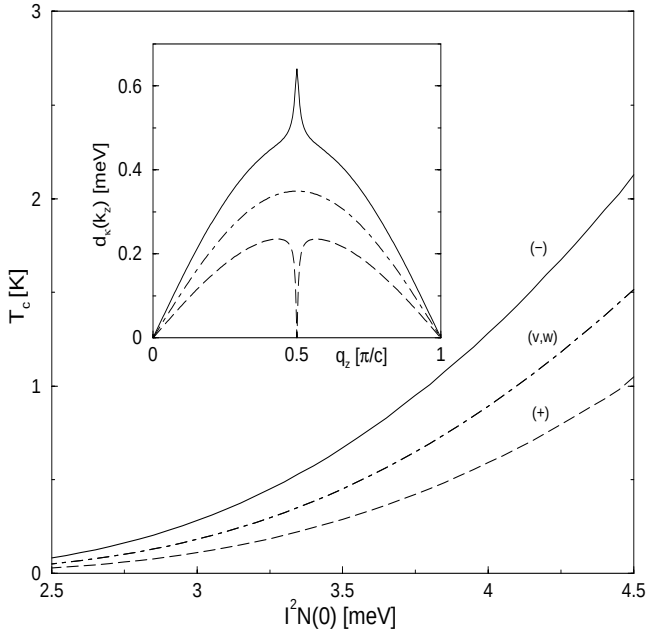

Fig. 9. Variation of transition temperature with coupling strength $\Delta\lambda_{sc} = I^2N(0)$ for the (v, w) odd parity doublet states. With AF order effect suppressed ($(\lambda_{AF} \equiv 0)$ T_c's are degenerate (dash-dotted line). With effect of λ_{AF} (Eq. (97)) included a splitting appears (full and dashed lines). Therefore in the presence of AF only the nondegenerate $d_-(k_z)$ state of equation (99) will be stable at any temperature below $T_c^v = 1.8$ K for $\Delta\lambda_{sc} = 4.3$ meV. *Inset:* wave number (k_z)-dependence of the gap functions $d_\pm(k_z)$ and $d_{v,w}(k_z)$ $(\lambda_{AF} \equiv 0)$ at $T = 0.05$ K. The anomalies at the Bragg plane $\frac{1}{2}Q_z = \frac{\pi}{2c}$ are due to the effect of AF order.

will appear. The k_z-dependence of $d_\pm^{\mathbf{k}}$ and $d_{(v,w)}^{\mathbf{k}}$ $(\lambda_{AF} \equiv 0)$ is illustrated in Figure 9 (inset). Here $\Delta\lambda_{sc} = 4.3$ meV $(\lambda_{sc} = 0.72)$, which after equation (98) corresponds to $\lambda_{AF} = 0.018$, is fixed to reproduce the physical value for $T_c = 1.8$ K for $d_-^{\mathbf{k}}$.

6 A hybrid model including spin fluctuations

It has been the aim of the previous analysis to investigate a new type of pairing mechanism which is a consequence of the dual nature of $5f$-electron in UPd_2Al_3. The model employed in equation (1) as an extreme case without any repulsion ($I_c = 0$) between $5f$-conduction electrons of the type given in equation (34). Therefore only the new pairing mechanism *via* the exchange of magnetic excitons is possible which was then studied for its own sake. In a real $5f$-compound one has to take into account also the quasiparticle Coulomb repulsion ($I_c > 0$) described by equation (34) which leads to a conventional spin fluctuation type part for the total pairing potential. In the present model approach one cannot decide on a purely theoretical basis which mechanism is the most important one. In this last section we therefore study a hybrid model where both contributions are simply added, neglecting any cross influence. We investigate the evolution of the pair potential and favorable sc states as a function of the ratio $\rho = (I_c/I)$ which controls the relative strength of these contributions. The pure magnetic exciton model studied before corresponds to $\rho = 0$. The two contributions of equations (34, 43) to the total pair potential are determined by the RPA static conduction electron susceptibility $\chi(\mathbf{q})$ and the exciton mode energy $\omega_-(\mathbf{q})$ respectively. Due to equations (55, 56) they are related *via*

$$I^2\chi_0(\mathbf{q}) = -[\omega_-(\mathbf{q}) + \alpha^2\langle S\rangle J'_{ff}(\mathbf{q})] + \omega_0 \tag{100}$$

with $\omega_0 = \Delta' + I^2\bar{\chi}$, $\bar{\chi} = \frac{1}{N}\sum_{\mathbf{q}}\chi(\mathbf{q})$. Since the superexchange $J'_{ff}(\mathbf{q})$ is unknown we restrict to the simplest possible case assuming $J'_{ff}(\mathbf{q}) \simeq 0$, then $\chi_0(\mathbf{q})$ is directly determined by the magnetic exciton dispersion $\omega_-(\mathbf{q})$ up to a constant ω_0 which has to satisfy the constraint

$$I^2\chi_0(\mathbf{q}) = \omega_0 - \omega_-(\mathbf{q}) \geq 0. \tag{101}$$

Then, using equations (38, 58) the total pair potential of the hybrid model is given by

$$\begin{aligned} V_s &= I^2\left[\frac{3}{2}\rho^2\chi(\mathbf{q}) + \frac{1}{\omega_R(\mathbf{q})}\right] \\ V_u &= -I^2\left[\frac{1}{2}\rho^2\chi(\mathbf{q}) - \frac{1}{\omega_-(\mathbf{q})}\right] \\ V_v = V_w &= -I^2\left[\frac{1}{2}\rho^2\chi(\mathbf{q}) + \frac{1}{\omega_-(\mathbf{q})}\right] \end{aligned} \tag{102}$$

where the RPA conduction electron susceptibility of equation (39) is obtained as

$$\rho^2\chi(\mathbf{q}) = \frac{(\frac{\rho}{I})^2[\omega_0 - \omega_-(\mathbf{q})]}{1 - \frac{\rho}{I}[\omega_0 - \omega_-(\mathbf{q})]}\,. \tag{103}$$

For the hybrid model of equation (102) one can now calculate the q_x, q_y-averaged potentials $V_\kappa(q_z)$ as in equation (71) where the bar will now be suppressed. They are shown in Figure 10 as function of q_z for parameters ω_0, ρ chosen such that equation (101) is fulfilled and $\chi(\mathbf{q})$ stays paramagnetic, *i.e.* nonsingular. One observes that the singlet potential (V_s) has now also a pronounced maximum at $\mathbf{Q}$ comparable to the potentials $V_{v,w}$ for the odd parity doublet state. Note that for the hybrid model $V_u \neq -V_{v,\,w}$ and therefore three potential functions are present in Figure 10 contrary to the situation in the pure magnetic exciton model of Figure 6. The stability of the singlet sc state should now be increased as ρ increases. This can clearly be seen by plotting the relevant Fourier components V_κ^m as function of increasing ρ, *i.e.* increasing the spin fluctuation contribution to the pairing. This is done for the unstable singlet state in Figure 7 (dashed curve, $m = 1$) *versus* the two most favorable odd parity states (upper arrows in Figure 7) and the result is shown in Figure 10. For $\rho \geq 0.09$ one has $-V_s > 0$ and the singlet state becomes possible. For even larger $\rho \geq 0.12$ it becomes more stable than the $d_u(\mathbf{k})$ $(m = 2)$ odd parity state and then $-V_s$ rapidly approaches the potentials $V_{v,\,w}$ for the doublet state for the largest value of ρ. At this value the

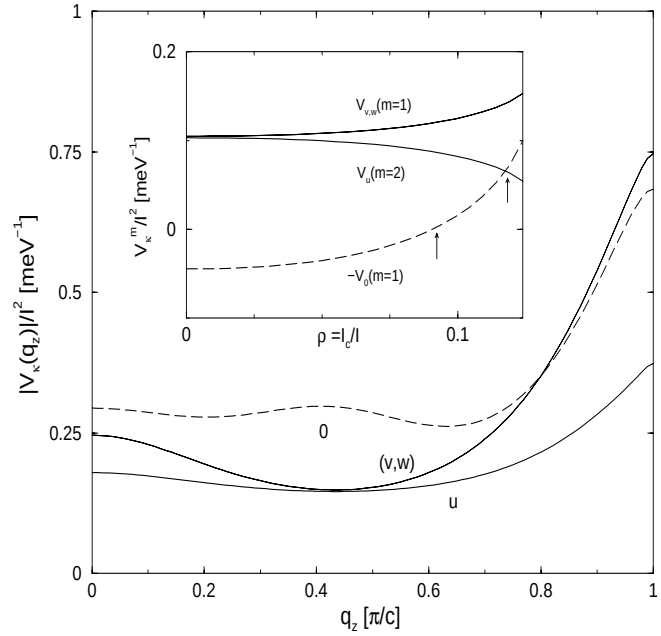

Fig. 10. Effective pair potentials (absolute values) for the hybrid model for even (0) and odd (u, v, w) parity for $\rho = I_c/I = 0.124$. *Inset:* most important Fourier components as function of model parameter ρ. With increasing ρ (increasing spin fluctuation contribution) the even parity singlet ($\kappa = 0$, $m = 1$) becomes stable at $\rho = 0.097$ (first arrow) and then more favorable than the odd parity u state (second arrow) but stays less favorable than the (v, w) odd parity doublet up to the maximum $\rho = 0.124$.

model $\chi(\mathbf{q})$ in equation (101) becomes singular indicating an AF instability of the conduction electron system. For the hybrid model with $J'_{ff}(\mathbf{q}) = 0$ and $\chi(\mathbf{q})$ given by equation (103) the odd parity state is therefore always the stable one, however the singlet state $d_0(k_z)$ becomes increasingly favorable as the spin fluctuation part increases. In principle it is possible that in the general case with the (unknown) $J'_{ff}(\mathbf{q})$ included in equation (100) the hybrid model will prefer the singlet sc state $d_0(\mathbf{k})$. Of course, if we neglect the magnetic exciton part altogether and consider only the isotropic pure spin fluctuation model then according to equation (38) $V_s \equiv V_0 = -3V_{u,\,v,\,w}$, and provided $\chi(\mathbf{q})$ has the maximum at $\mathbf{q} = \mathbf{Q}$, the singlet even parity sc state $d_0(k_z) = d_0^1 \cos k_z$ is the stable one.

7 Summary and outlook

In this work a dual model of localised and itinerant $5f$-electrons was studied as a generic model for superconductivity in uranium-compounds and applied to UPd_2Al_3. The dual nature of $5f$-electrons in this compound was concluded from experimental evidence, notably susceptibility and normal state Knight shift measurements. The localized electrons were assumed to be in a $5f^2$ configuration split by the CEF into singlet ground and excited states separated by an energy $\Delta = 6$ meV. The conduction electrons form band states whose main FS sheet can be described by a corrugated cylinder aligned along the c-axis. Due to RKKY and superexchange interactions the CEF excitation at Δ is broadened into a dispersive band of magnetic excitons which become soft at the Néel temperature T_N where an induced AF moment appears in the singlet ground state. These magnetic excitons where found in inelastic neutron scattering experiments [10–12] and a theoretical explanation of their dispersion has been given within the AF singlet ground state model. Furthermore a comparison with tunneling experiments [17] has suggested that the exchange of magnetic excitations between conduction electrons leads to a new type of pairing mechanism which is responsible for superconductivity in UPd_2Al_3. The consequences of this hypothesis have been analyzed in detail within the dual model. The new magnetic exciton mediated pair potential was derived within a diagrammatic RPA type approach and compared to the results of the well known spin fluctuation theory pair potential caused by anti-paramagnon exchange. It was found that the former manifestly violates rotational symmetry in spin space contrary to the latter which is composed of spin singlet and triplet contributions due to rotational invariance. The new effective pair potential due to magnetic exciton exchange has a lower symmetry with contributions from the even singlet, another odd parity nondegenerate and an odd parity doublet contribution. The projector representation defining the irreducible pair potentials has been derived and for the cylindrical FS sheet the effectively 1D gap equations have been solved. The favoured representation is determined by the largest Fourier coefficient of the in-plane averaged pair potential. In case of AF magnetism is excluded it was found that the new mechanism favors the odd parity doublet state which has equatorial node lines in the gap function. The singlet state is generally not favored in the present weak coupling version of the magnetic exciton mechanism. The influence of singlet ground state AF on sc leads to important consequences: The doublet state is strongly split and the stable sc state is a nondegenerate odd parity state given by equation (99).

A hybrid model including spin fluctuations has also been considered. In the simplified case that superexchange between localized $5f$-electrons can be neglected the spin fluctuation pair potential can also be obtained from the magnetic exciton dispersion. As expected its admixture leads to a stabilization of the singlet pair state with node lines at $\pm\frac{1}{2}\mathbf{Q}$. However within the simplified model the above mentioned odd parity state remains the sc ground state. In a more general hybrid model which does not have a direct connection between the two contributions to the pair potential an even singlet sc ground state is possible which is favored for the pure spin fluctuation model of the pair potential. In this work the thermodynamic signatures of the proposed and possible gap functions have not been discussed. Their detailed investigation is an important aspect for future work.

Thermal conductivity measurements [28,29] point to the existence of node lines in the gap in a plane

parallel to the hexagonal ab plane but so far do not allow to give their position ck_z along the c axis. Recently it has been proposed [30,31] that the field-angle dependence of thermal conductivity gives a unique possibility to determine the position of the node lines. It has been shown [31] that the angle dependence should be distinctly different for an odd parity gap function $\sin k_z$ with $k_z = 0$ node line as in equation (79) and the even parity gap function $\cos k_z$ with node line at $k_z = \frac{\pi}{2}$ as in equation (80). It is generally believed that the observation of a Knight shift below T_c [9,32,33] points to an singlet even parity gap function as in equation (80) which is not favored by the present form of the magnetic exciton model. However the Knight shift is also strongly influenced by the AF ordered localised moments and the quantitative extraction of the itinerant part is not unique. Therefore one has to await the field-angle dependent thermal conductivity measurements to solve the problem of the true node line position and parity of the order parameter.

The theory developed in this paper investigates the basic mechanism of Cooper pair formation *via* the magnetic exciton exchange in U-compounds with dual (localised and itinerant) $5f$-electrons. In its context differences to the conventional spin fluctuation mechanism and general properties of the nonretarded pair potentials were analyzed. The complete separation of $5f$-electrons into localised and itinerant parts in the dual model is to some degree artificial and needs to be refined. Also one cannot expect fully quantitative predictions for UPd_2Al_3 from the present simplified weak coupling approach. Ultimately a strong coupling theory with a retarded magnetic exciton mediated pair potential and inclusion of a more realistic FS is necessary. This will also necessitate a fully numerical treatment of the gap equations to investigate the new pairing mechanism for UPd_2Al_3 and the question of the most favorable symmetry for the gap function.

The author would like to thank K. Maki, N. Sato, R. Shiina, A.N. Yaresko and G. Varelogiannis for useful discussions.

Appendix A

In this appendix we give the basic geometry of the conventional unit cells in the direct (Wigner Seitz cell: WS) and reciprocal (Brillouin zone: BZ) hexagonal lattice for the discussion of the magnetic exciton dispersion. The BZ is rotated by 30° with respect to the WS cell. The relevant primitive lattice vectors of the direct and reciprocal lattices are given, respectively, by

$$\begin{aligned}\mathbf{a} &= a\left(\frac{1}{2}, -\frac{\sqrt{3}}{2}, 0\right)\\ \mathbf{b} &= a\left(\frac{1}{2}, \frac{\sqrt{3}}{2}, 0\right)\\ \mathbf{b} &= c(0,0,1)\end{aligned} \tag{A.1}$$

$$\begin{aligned}\mathbf{a}^* &= \frac{2\pi}{a}\left(1, -\frac{1}{\sqrt{3}}, 0\right)\\ \mathbf{b}^* &= \frac{2\pi}{a}\left(1, \frac{1}{\sqrt{3}}, 0\right)\\ \mathbf{b}^* &= \frac{2\pi}{c}(0,0,1).\end{aligned} \tag{A.2}$$

Any wave vector can be written in this basis as $\mathbf{q} = h\mathbf{a}^* + k\mathbf{b}^* + l\mathbf{c}^*$. In reduced units of $\frac{1}{a}$ and $\frac{1}{c}$, $\mathbf{q}$ is then given by

$$\begin{aligned}\text{PMBZ}: \ \mathbf{q} &= 2\pi\left(h+k, \frac{1}{\sqrt{3}}(h-k), l\right)\\ \text{AFBZ}: \ \mathbf{q}' &= 2\pi\left(h+k, \frac{1}{\sqrt{3}}(h-k), \frac{1}{2}l'\right).\end{aligned} \tag{A.3}$$

For the q_z components the relation $l' = 2l - 1$ or $l = \frac{1}{2}(l'+1)$ holds, *i.e.* the AFBZ is obtained from the PMBZ through the shift by an AF wave vector $\mathbf{Q} = (0,0,\pi)$ and scaling by a factor $\frac{1}{2}$. The corresponding wave vectors $\mathbf{q}' = \mathbf{q} - \mathbf{Q}$ of the symmetry points of the hexagonal AFBZ are then given by

$$\begin{aligned}\Gamma &: \pi(0,0,0)\\ M &: \pi\left(1, -\frac{1}{\sqrt{3}}, 0\right)\\ K &: \pi\left(\frac{4}{3}, 0, 0\right)\\ A &: \pi\left(0,0,\frac{1}{2}\right)\\ A' &: \pi(0,0,1)\\ L &: \pi\left(1, -\frac{1}{\sqrt{3}}, \frac{1}{2}\right)\\ H &: \pi\left(\frac{4}{3}, 0, \frac{1}{2}\right).\end{aligned}$$

In the AFBZ the symmetry point A′ is equivalent to Γ since it is shifted by a reciprocal lattice vector $\mathbf{Q}$.

Appendix B

The single-ion susceptibility tensor $\overleftrightarrow{u}(\omega)$ which is a necessary ingredient for the calculation of the magnetic exciton dispersion from equation (18) is obtained from the general linear response expression for two operators A, B in a system of two levels $\epsilon_\pm$ corresponding to CEF singlet eigenstates $|\pm\rangle$ in the molecular field:

$$\begin{aligned}u_{BA}(\omega) &= P(T)\left[\frac{M_{BA}^{+-}}{\Delta' + \omega} + \frac{M_{BA}^{-+}}{\Delta' - \omega}\right]\\ P(T) &= 2\langle S\rangle = \tanh\frac{\beta}{2}\Delta'\\ M_{BA}^{\alpha\beta} &= \langle\alpha|\hat{B}|\beta\rangle\langle\beta|\hat{A}|\alpha\rangle.\end{aligned} \tag{B.1}$$

Here $\langle S\rangle \equiv \langle S_z\rangle$, $\Delta' = \epsilon_+ - \epsilon_-$ is the CEF excitation energy of equation (12), $\alpha, \beta = \pm$ refer to the

mf-eigenstates in the ordered phase (Eq. (11)) and $\hat{A} = A - \langle A\rangle$, $\hat{B} = A - \langle B\rangle$. For $A,\ B = J_\alpha$ ($\alpha = x,\ y,\ z$) the form of the 3×3 dipolar Cartesian susceptibility tensor $\overleftrightarrow{u}(\omega)$ is too cumbersome for solving the secular equation for the exciton modes. This may be remedied by performing a real space rotation $(x,\ y,\ z) \rightarrow (x',\ y,\ z')$ around the y-axis by an angle θ_r such that it exactly compensates the effect of the rotation in state space which transforms to the eigenstates $|\pm\rangle$ of the mf-Hamiltonian equation (11). In this basis one has

$$\begin{aligned}\tilde{J}_x &= \frac{1}{2}\alpha \begin{pmatrix} -b & a \\ a & b \end{pmatrix} \\ \tilde{J}_y = J_y &= \frac{1}{2}\alpha \begin{pmatrix} 0 & -\mathrm{i} \\ \mathrm{i} & 0 \end{pmatrix} \\ \tilde{J}_z &= \frac{1}{2}\alpha \begin{pmatrix} a & b \\ b & -a \end{pmatrix} \end{aligned} \tag{B.2}$$

with $a = \cos 2\theta = [1+\gamma'^2]^{-\frac{1}{2}}$, $b = \sin 2\theta = \gamma' a$. Performing the counter- rotation leads to ($u_r = \cos\theta_r,\ v_r = \sin\theta_r$)

$$J'_x = u_r \tilde{J}_x - v_r \tilde{J}_z,\ J'_y = \tilde{J}_y,\ J'_x = u_r \tilde{J}_x - v_r \tilde{J}_z \tag{B.3}$$

defining $\phi = 2\theta$ this can be written

$$\begin{aligned} J'_x &= \frac{1}{2}\alpha \begin{pmatrix} -\sin(\theta_r+\phi) & \cos(\theta_r+\phi) \\ \cos(\theta_r+\phi) & \sin(\theta_r+\phi) \end{pmatrix} \\ J'_y = J_y &= \frac{1}{2}\alpha \begin{pmatrix} 0 & -\mathrm{i} \\ \mathrm{i} & 0 \end{pmatrix} \\ J'_z &= \frac{1}{2}\alpha \begin{pmatrix} \cos(\theta_r+\phi) & \sin(\theta_r+\phi) \\ \sin(\theta_r+\phi) & -\cos(\theta_r+\phi) \end{pmatrix}. \end{aligned} \tag{B.4}$$

By choosing $\theta_r \equiv -\phi = -2\theta$ the two transformations compensate and $J'_x = J_x$, $J'_y = J_y$, $J'_z = J_z$. Therefore in the rotated (x', y', z')-coordinate system the susceptibility tensor of the AF ordered two level system is identical to the same tensor for the paramagnetic case in the original (x, y, z) hexagonal coordinate system. It has only nonzero elements for x, y and is given by

$$\begin{aligned} \overleftrightarrow{u}'(\omega) &= \frac{\alpha^2\langle S\rangle}{\Delta'^2 - \omega^2} \begin{pmatrix} \Delta' & \mathrm{i}\omega \\ -\mathrm{i}\omega & \Delta' \end{pmatrix} \\ \overleftrightarrow{u}^{-1'}(\omega) &= \frac{1}{\alpha^2\langle S\rangle} \begin{pmatrix} \Delta' & -\mathrm{i}\omega \\ \mathrm{i}\omega & \Delta' \end{pmatrix}. \end{aligned} \tag{B.5}$$

This form will be used in the secular equation (20).

References

1. M. Sigrist, K. Ueda, Rev. Mod. Phys. **63**, 239 (1991).
2. R. Fisher, S. Kim, B. Woodfield, N. Phillips, L. Taillefer, K. Hasselbach, J. Flouquet, A. Giorgi, J.L. Smith, Phys. Rev. Lett. **62**, 1411 (1989).
3. G. Bruls, D. Weber, B. Wolf, P. Thalmeier, B. Lüthi, A. de Visser, A.A. Menovsky, Phys. Rev. Lett. **65**, 2294 (1990).
4. F. Kromer, R. Helfrich, M. Lang, F. Steglich, C. Langhammer, A. Bach, T. Michels, J.S. Kim, G.R. Stewart, Phys. Rev. Lett. **81**, 4476 (1998).
5. H. Amitsuka, M. Sato, N. Metoki, M. Yokoyama, K. Kuwahara, T. Sakakibara, H. Morimoto, S. Kawarazaki, Y. Miyako, J.A. Mydosh Phys. Rev. Lett. **83**, 5114 (1999).
6. Ch. Geibel, C. Schank, S. Thies, H. Kitazawa, C.D. Bredl, A. Böhm, M. Rau, A. Grauel, R. Caspary, R. Helfrich, U. Ahlheim, G.Weber, F. Steglich, Z. Phys. B **84**, 1 (1991).
7. G. Zwicknagl, A.N. Yaresko, P. Fulde, Phys. Rev. B **65**, 081103(R) (2002).
8. R. Grauel, A. Böhm, H. Fischer, C. Geibel, R. Köhler, R. Modler, C. Schank, F. Steglich, G. Weber, T. Komatsubara, N. Sato, Phys. Rev. B **46**, 5818 (1992).
9. R. Feyerherm, A. Amato, F.N. Gygax, A. Schenck, C. Geibel, F. Steglich, N. Sato, T. Komatsubara, Phys. Rev. Lett. **73**, 1849 (1994).
10. T.E. Mason, G. Aeppli, Matematisk-fysiske Meddelelser **45**, 231 (1997).
11. N. Bernhoeft, N. Sato, B. Roessli, N. Aso, A. Hiess, G.H. Lander, Y. Endoh, T. Komatsubara, Phys. Rev. Lett. **81**, 4244 (1998).
12. N.N. Sato, N. Aso, G.H. Lander, B. Roessli, T. Komatubara, Y. Endoh, J. Phys. Soc. Jpn **66**, 1884 (1997); **66**, 2981 (1997).
13. N. Bernhoeft, Eur. Phys. J. B **13**, 685 (2000).
14. M. Jourdan, M. Huth, H. Adrian, Nature **398**, 47 (1999).
15. N.K. Sato, N. Aso, K. Miyake, R. Shiina, P. Thalmeier, G. Varelogiannis, C. Geibel, F. Steglich, P. Fulde, T. Komatsubara, Nature **410**, 340 (2001).
16. R. Shiina, private communication.
17. M. Jourdan, M. Huth, H. Adrian, Nature 398, **47** (1999).
18. N.K. Sato, N. Aso, K. Miyake, R. Shiina, P. Thalmeier, G. Varelogiannis, C. Geibel, F. Steglich, P. Fulde, T. Komatsubara, Nature **410**, 340 (2001).
19. K. Knöpfle, A. Mavromaras, L.M. Sandraatski, J. Kübler, J. Phys. Cond. Matter **8**, 901 (1996).
20. Y. Inada, H.Yamagami, Y. Haga, K. Sakurai, Y. Tokiwa, T. Honma, E. Yamamoto, Y. Onuki, T. Yanagisawa, J. Phys. Soc. Jpn **68**, 3643 (1999).
21. J. Jensen, A.R. Mackintosh, *Rare Earth Magnetism, Structures and Excitations* (Clarendon Press, Oxford, 1991).
22. A. Krimmel, P. Fischer, B. Roessli, H. Maletta, C. Geibel, C. Schank, A. Grauel, A. Loidl, F. Steglich, Z. Phys. B **86**, 161 (1986).
23. S. Nakajima, Prog. Theor. Phys. **50**, 1101 (1973).
24. K. Miyake, S. Schmitt-Rink, C.M. Varma, Phys. Rev. B **34**, 6554 (1986).
25. A.I. Morosov, JETP **83**, 1048 (1996).
26. A. Amici, P. Thalmeier, P. Fulde, Phys. Rev. Lett. **84**, 1800 (2000).
27. A. Amici, P. Thalmeier, P. Fulde, Physica C **317-318**, 471 (1999).
28. M. Chiao, B. Lussier, B. Ellman, L. Taillefer, Physica B **230-232**, 370 (1997).
29. M. Hiroi, M. Sera, N. Kobayashi, Y. Haga, E. Yamamoto, Y. Onuki, J. Phys. Soc. Jpn **66**, 1595 (1997).
30. Y. Sun, K. Maki, Europhys. Lett. **32**, 355 (1995).
31. P. Thalmeier, K. Maki, Europhys. Lett. **58**, 119 (2002).
32. H. Tou, Y. Kitaoka, K. Asayama, C. Geibel, C. Schank, F. Steglich, J. Phys. Soc. Jpn **64**, 725 (1995).
33. K. Matsuda, Y. Kohori, T. Kohara, Phys. Rev. B **55**, 15223 (1997).